



OPEN In-vitro assessment of anti-breast cancer potential of pumpkin seed oil nanoemulsion with mechanistic insights into cytotoxicity and apoptosis

Rupali Ghosh, Noor Fatima, Abul Vafa, Syed Abuzar Raza Rizvi & Saima Wajid✉

Breast cancer is the most prevalent malignancy in women with 16% of all cancer deaths and current therapies frequently resulting in significant adverse consequences. Pumpkin seed oil (PSO) possesses antibacterial, antiviral, cytotoxic, and anticancer effects. Nonetheless, its hydrophobic characteristics restrict bioavailability, which can be enhanced by a nanoemulsion system. The optimization of pumpkin seed oil nanoemulsion (PSO-NE) was affected by surfactant concentration and sonication duration, resulting in a droplet size of 152.0 nm, PDI of 0.189 and Zeta Potential of -23.5 mV. PSO-NE displayed dose-dependent cytotoxicity, revealing a significantly decreased IC_{50} compared to free PSO and Doxorubicin after 24 h of exposure ($p < 0.01$). At IC_{50} concentration (MCF-7 = 46.6 μ g/ml and MDA-MB-231 = 60 μ g/ml) PSO-NE significantly elicited morphological alterations, decreased cell proliferation, enhanced phosphatidylserine exposure, and halted the cell cycle ($p < 0.001$). The expression of genes (Bcl-2, STAT-3, and NF- κ B), associated with cell proliferation, was significantly downregulated ($p < 0.001$), while the expression of genes (p53, Bax, and caspase 3), linked to apoptosis, was significantly upregulated compared to the untreated cell lines ($p < 0.001$), indicating the activation of apoptotic gene expression. The targeted cytotoxicity of PSO-NE against breast cancer and its ability to induce apoptosis and cell cycle arrest, underscores a promising anticancer drug.

Keywords Pumpkin seed oil nanoemulsion, Ultrasonication, Cytotoxic potential, Cell cycle arrest, Apoptotic gene expression, Anticancer

This century is poised to witness cancer emerging as the foremost cause of death within the population, currently positioned as the leading cause of mortality following cardiovascular diseases. Nevertheless, the economic implications of cancer persist in generating significant disparities in the accessibility of innovative cancer treatments across nations¹. Despite ongoing technological progress, breast cancer remains the second most prevalent and lethal disease among women². In 2020, breast cancer overtook lung cancer as the leading cause of cancer prevalence globally³. In the female population, breast cancer accounts for approximately 25% of all cancer diagnoses and 16% of cancer-related fatalities^{4,5}. Breast cancer encompasses physiologically distinct subgroups, each exhibiting varying degrees of responsiveness to diverse therapeutic approaches and clinical outcomes. The presence of estrogen receptors (ERs), progesterone receptors (PRs), and the human epidermal growth factor receptor 2 (HER2) is commonly employed to classify invasive breast cancer⁶.

The primary constraints of the already employed therapy encompass the potential for relapse, exorbitant expenses, unfavorable outcomes, non-specific targeting, and the emergence of medication resistance^{7,8}. The anticancer medications utilized shown significant toxicity not only towards the malignant cells, but also towards the healthy cells of the affected region. Therefore, it is essential to develop alternatives that provide comparable or higher therapeutic efficacies, demonstrate greater cost-effectiveness, and comply with the utilization of natural compounds^{9,10}. Presently, researchers are exploring natural plants-derived compounds in their quest to discover innovative anticancer medications¹¹.

Pumpkin is one such plant that is commonly consumed as both food and traditional medicine for extended periods of time. The pumpkin, *Cucurbita maxima* Duchesne belongs to the genus *Cucurbita* and family

Department of Biotechnology, School of Chemical and Life Sciences, Jamia Hamdard, Hamdard Nagar, New Delhi 110062, India. ✉email: swajid@jamiahamdard.ac.in

*Cucurbitaceae*¹². Pumpkin is indigenous to the plateaus of central and South America, but is cultivated throughout the World¹³. Numerous in vitro and in vivo studies utilizing crude pumpkin fruit extract and different purified fractions, such as proteins and carbohydrates, have demonstrated anticancer effects towards melanoma, Ehrlich ascites carcinoma and leukemia¹⁴. In recent times, there has been a growing interest in the intake of pumpkin seed oil (PSO) due to several studies linking it to various health benefits. PSO is a highly abundant and natural reservoir of triterpenes, phytosterols, phytoestrogens, antioxidative phenolic compounds, polyunsaturated fatty acids, tocopherol, and carotenoids¹⁵. In addition, the antioxidant, hypoglycemic, and hypolipidemic properties have also been reported¹⁶. PSO has been documented to possess therapeutic potential for hypertension, atherosclerosis, prostatic hypertrophy, and urinary bladder hyperplasia^{17–19}. Numerous research studies have demonstrated that PSO can trigger apoptosis, impede cell proliferation, and decrease tumor growth in multiple cancer models, including breast and prostate malignancies^{20,21}.

The poor biocompatibility, bioavailability, and solubility of PSO in the bloodstream have restricted its potential therapeutic utility. Nanotechnology systems have been created to optimize biocompatibility and accessibility by nano-emulsification processes²². Out of all devised drug delivery systems, nanoemulsions have emerged as a promising & efficient drug delivery system for various chemotherapeutics/ bioactive drugs because of nanoemulsion's distinctive and unique qualities, such as biocompatibility, bioavailability, biodegradable, nanometric sizes, large surface areas, longer circulation half-life, enhanced permeable retention (EPR), formulation ease, thermodynamic stability, and enhancing phyto-compounds solubility and bioavailability^{23,24}. Nanoemulsions can be created utilizing components sanctioned by the Food and Drug Administration (FDA), so significantly ensuring their safety characteristics. Nanoemulsions (NE) consist of small droplets, typically up to 200 nm in size, distributed in either water-based or hydrophobic solutions^{7,25}. Various studies illustrate therapeutic activities of PSO-NE against benign prostatic hyperplasia, steatohepatitis, and peptic ulcer^{26–28}. The anticancer efficacy of PSO-NE against breast cancer has not yet been assessed.

A therapeutic drug regulates cancer cells by many pathways, including apoptosis, necrosis, and autophagy. Apoptosis is the most often employed mechanism for eliminating cancer cells in all these approaches. The induction of apoptosis is an efficient strategy for eradicating cancer cells. To evaluate a drug's potential for inducing apoptosis, it is essential to first ascertain its cytotoxicity²⁹. Thus, the main objective of the current study was to formulate and characterize pumpkin seed oil nanoemulsion (PSO-NE) and evaluate the cytotoxic and apoptotic potential of the formulated PSO-NE against breast cancer cell lines (MCF-7 and MDA-MB-231).

Results
Identification of pumpkin seed oil active compounds by GC–MS

PSO is a complex mixture containing bioactive compounds such as phytosterols, tocopherols, and unsaturated fatty acids. The predominant fatty acids in pumpkin seed oil are linoleic (50.7%), oleic (18.8%), palmitic (17.9%), and stearic (12.4%). The GC–MS chromatogram had showed 19 active compounds present in the PSO as shown in Table 1 (Supplementary Table S1). GC–MS reported 9, 12-Octadecadienoic acid (z,z)- as the constituent with highest peak area % of 37.41 followed by Hexadecanoic acid, methyl ester (28.28%), Methyl stearate (14.41%), 9-Octadecenoic acid, methyl ester, (e)- (6.10%), Squalene (2.68%), and Hexadecadienoic acid, methyl ester (2.13%) as shown in Fig. 1 (Supplementary Figure S1).

Peak	R. time	Area	Area%	Name	Formula
1	11.612	2,000,025	0.39	Methyl tetradecanoate	C ₁₅ H ₃₀ O ₂
2	16.156	2,632,245	0.52	9-Hexadecenoic acid, methyl ester, (z)-	C ₁₇ H ₃₂ O ₂
3	16.955	143,231,454	28.28	Hexadecanoic acid, methyl ester	C ₁₇ H ₃₄ O ₂
4	18.583	1,718,914	0.34	(z)-Methyl heptadec-9-enoate	C ₁₈ H ₃₄ O ₂
5	19.192	3,318,955	0.66	Heptadecanoic acid, methyl ester	C ₁₈ H ₃₆ O ₂
6	21.404	189,480,714	37.41	9,12-Octadecadienoic acid (z,z)-	C ₁₈ H ₃₂ O ₂
7	21.531	30,891,427	6.10	9-Octadecenoic acid, methyl ester, (e)-	C ₁₉ H ₃₆ O ₂
8	21.839	73,014,271	14.41	Methyl stearate	C ₁₉ H ₃₈ O ₂
9	24.615	10,810,441	2.13	Hexadecadienoic acid, methyl ester	C ₁₇ H ₃₀ O ₂
10	24.709	1,048,291	0.21	Oxiraneoctanoic acid, 3-oxetyl-, methyl ester, trans-	C ₁₉ H ₃₆ O ₃
11	25.091	2,540,513	0.50	9-Octadecenoic acid, 12-hydroxy-, methyl ester, [r-(z)]-	C ₁₉ H ₃₆ O ₃
12	25.228	2,898,345	0.57	Cis-11-eicosenoic acid, methyl ester	C ₂₁ H ₄₀ O ₂
13	25.835	15,227,745	3.01	Eicosanoic acid, methyl ester	C ₂₁ H ₄₂ O ₂
14	26.732	3,695,714	0.73	1,1,4a,7-Tetramethyl-2,3,4,4a,5,6,7,8-octahydro-1 h-benzo[a]cyclohepten	C ₁₅ H ₂₆ O
15	28.494	664,727	0.13	Cyclopropaneoctanoic acid, 2-[[2-[(2-ethylcyclopropyl)methyl]cyclopropyl]methyl]-, methyl	C ₂₂ H ₃₈ O ₂
16	29.821	7,019,475	1.39	Docosanoic acid, methyl ester	C ₂₃ H ₄₆ O ₂
17	31.733	451,671	0.09	Tricosanoic acid, methyl ester	C ₂₄ H ₄₈ O ₂
18	33.553	2,322,811	0.46	Tetracosanoic acid, methyl ester	C ₂₅ H ₅₀ O ₂
19	34.882	13,581,338	2.68	Squalene	C ₃₀ H ₅₀

Table 1. Compounds identified by GC–MS analysis of Pumpkin seed oil.

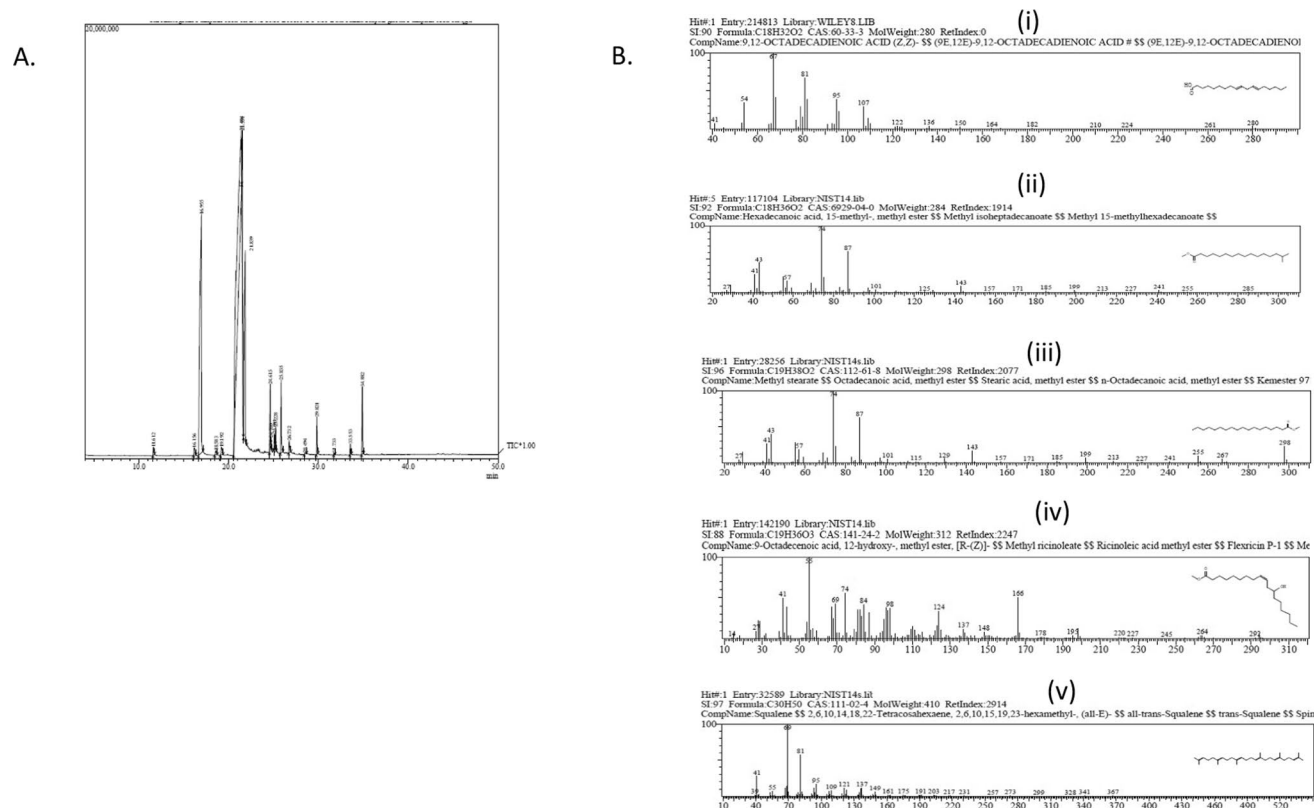


Fig. 1. (A) Chromatogram of GC-MS of the pumpkin seed oil (PSO). (B) Major compound identified in GC-MS analysis of the pumpkin seed oil (i) Octadecadienoic acid (z,z)- (ii) Hexadecanoic acid, methyl ester (iii) Methyl stearate (iv) 9-Octadecenoic acid, methyl ester (v) Squalene.

Formulation	Oil: Surfactant Ratio (v/v)	Sonication Time (mins)	Mean droplet size diameter (nm)	polydispersity index	Zeta potential (mV)
A1	1:1	10	300.15 ± 1.20	0.558 ± 0.002	- 34.5 ± 0.3
A2	1:2	10	251.60 ± 0.35	0.541 ± 0.007	- 36.4 ± 0.5
A3	1:3	10	238.50 ± 0.21	0.419 ± 0.001	- 32 ± 1.2
B1	1:1	15	289.32 ± 0.35	0.510 ± 0.003	- 32.25 ± 0.2
B2	1:2	15	232.51 ± 1.13	0.418 ± 0.007	- 32.15 ± 0.41
B3	1:3	15	205.63 ± 1.97	0.229 ± 0.004	- 30.4 ± 0.32
C1	1:1	20	253.61 ± 1.27	0.389 ± 0.005	- 29.3 ± 0.1
C2	1:2	20	217.87 ± 0.63	0.282 ± 0.008	- 25.7 ± 0.4
C3	1:3	20	154.91 ± 0.14	0.193 ± 0.008	- 24.3 ± 0.23

Table2. Varying concentrations of PSO-NE and their respective mean droplet size diameter, polydispersity index and Zeta potential.

Characterization of PSO-NE

DLS

To determine the optimized formulation, the characterization studies were performed on all preparations. Samples were prepared with varied oil to surfactant ratios (1:1, 1:2, and 1:3) and after sonication time of 10, 15, and 20 min were taken for characterization. The stability of the PSO-NE is determined by both the concentration of surfactant and the duration of sonication. As the sonication duration increased, a reduction in droplet size was observed, as detailed in Table 2. For example-for a sonication period of 10 min, droplet diameter of 300.15 ± 1.20 nm, 251.6 ± 0.35 nm, and 238.5 ± 0.21 nm was observed for oil: surfactant ratios of 1:1 (A1), 1:2 (A2), and 1:3 (A3) (v/v), respectively. With increasing the sonication duration to 15 min, the droplet sizes were further decreased to 289.32 ± 0.35 nm, 232.51 ± 1.13 nm, and 205.63 ± 1.97 nm for oil: surfactant ratios of 1:1 (B1), 1:2 (B2), and 1:3 (B3), respectively. Similarly, there was a corresponding reduction in droplet size when the sonication duration was extended to 20 min. Simultaneously, a decrease in droplet size was seen as the surfactant concentration increased. The maximum droplet size achieved was 253.6 ± 1.27 nm with an oil: surfactant ratio of 1:1 (6:6:88 v/v) after sonication for 20 min. By increasing the concentration of the surfactant to 1:2 (6:12:82 v/v)

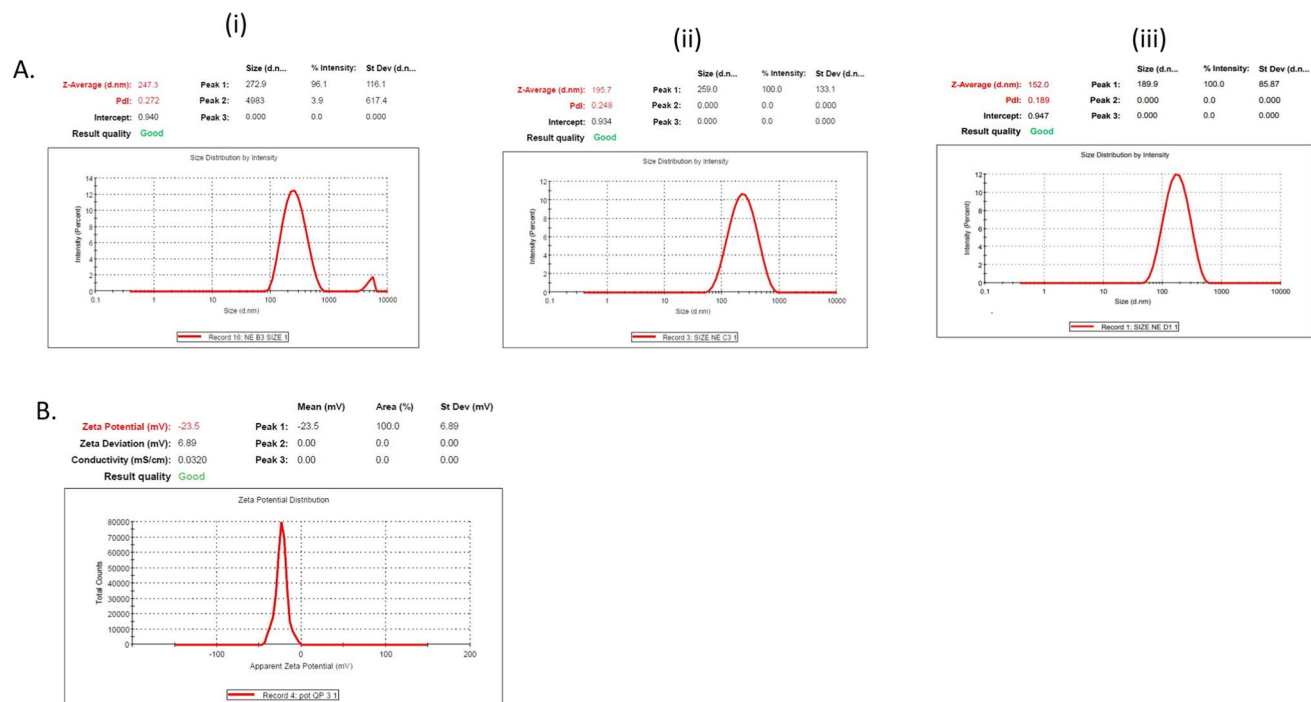


Fig. 2. Characterization of PSO-NE by DLS (A) The size distribution and PDI of the PSO-NE (i) C1 (1:1) (ii) C2 (1:2) (iii) C3 (1:3) after 20 min of sonication. (B) Zeta potential of the optimized PSO-NE (C3).

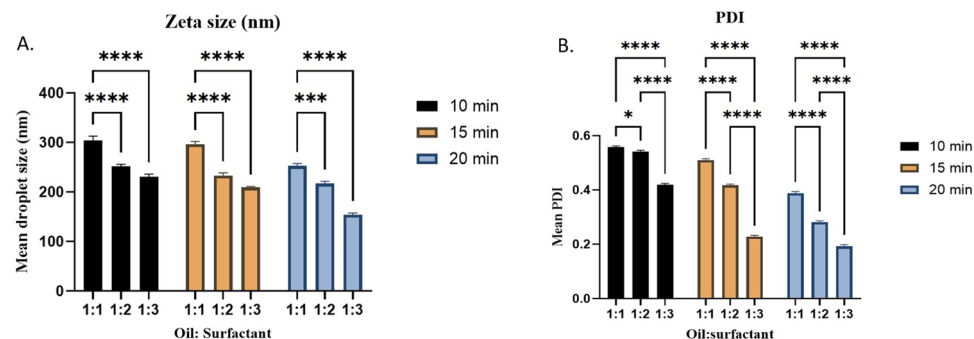


Fig. 3. (A) The mean droplet size of PSO-NE varies depending on the amount of oil to surfactant ratio and the duration of sonication. (B) The mean polydispersity index (PDI) of PSO-NE varies depending on the amount of oil to surfactant ratio and the duration of sonication. Data are representative of three experiments expressed as mean \pm SD ($n = 3$). * $P < 0.05$, ** $P < 0.01$, *** $P < 0.001$ using one way ANOVA Tukey post test.

and 1:3 (6:18:76 v/v), the size of the droplets decreased to a minimum of 217.6 ± 0.63 nm, and 154.9 ± 0.14 nm, respectively. Upon further amplification of the surfactant concentration, no notable decrease in droplet size was observed. Consequently, the PSO-NE was optimized to an oil-to-surfactant ratio of 1:3 (v/v) with sonication duration of 20 min (zeta size = 154.9 ± 0.14 and PDI = 0.193 ± 0.008), as observed in Figs. 2 and 3.

An increase in uniformity was observed as the surfactant concentration increased, resulting in a decrease in the polydispersity index. For instance, when the sonication time was 20 min, the polydispersity index was 0.389 ± 0.005 , 0.282 ± 0.008 , and 0.193 ± 0.008 for oil: surfactant ratios of 1:1, 1:2, and 1:3, respectively, as detailed in Fig. 2. The zeta potential provides an approximate measure of the surface charge of the particles in the nanoemulsion. Large magnitudes result in repulsive interactions between particles, which can enhance the physical stability of multiphase systems³⁰. For all the formulations, zeta potential is negatively charged and has high potential values. The value of zeta potential decreased with increase in surfactant concentration, indicate that further increase in surfactant will be destabilized the nanoemulsion system.

SEM and TEM

The scanning electron microscopy (SEM) pictures of PSO-NE showed droplets with irregular shapes, distinct contours, and visible cores. A little accumulation was noted. The transmission electron microscopy (TEM)

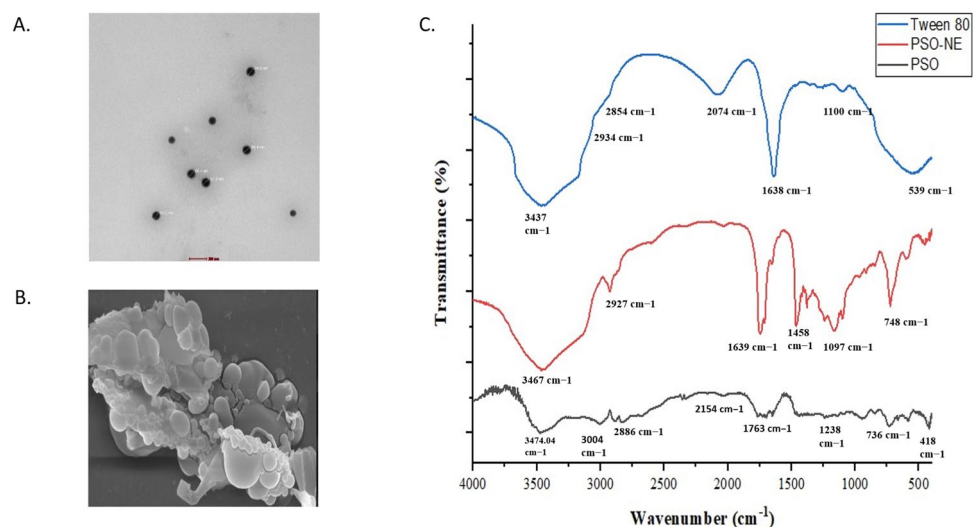


Fig. 4. Size and morphology of PSO-NE by (A) TEM, scale bar = 200 nm, (B) SEM, scale bar = 1 μm . (C) FT-IR spectra of PSO (Black), PSO-NE (Red), Tween 80 (Blue).

Formulation	Oil: Surfactant ratio (v/v)	Sonication Time (mins)	Absorbance (600 nm)	pH
A1	1:1	10	2.720	5.7
A2	1:2	10	2.680	5.8
A3	1:3	10	2.650	5.9
B1	1:1	15	2.702	5.8
B2	1:2	15	2.680	5.9
B3	1:3	15	2.647	6.0
C1	1:1	20	2.715	5.7
C2	1:2	20	2.600	5.9
C3	1:3	20	2.562	6.2

Table 3. Analysis and deductions of PSO-NE turbidity and pH investigations at different concentrations.

imaging revealed that the synthesized PSO-NE exhibited a spherical shape and were uniformly distributed with average size of 150 nm (Fig. 4). The diameters of the PSO-NEs were consistent with those observed using Dynamic Light Scattering (DLS).

FT-IR

The whole spectrum range of 4000–400 cm^{-1} clearly demonstrated the distinctions between the PSO and PSO-NE. The PSO spectra exhibited a prominent peak at 3474.04 cm^{-1} , which is likely attributed to the stretching of the OH group. The smaller, strong bands seen at 3004, 2886, and 2833 cm^{-1} are attributed to the stretching of the CH group. In the C=O stretching region of a saturated fat, there was a peak at 1763 cm^{-1} . The peaks at 1238, 1138, and 947 cm^{-1} are ascribed to the C–O–C stretching in aromatic acid esters and stretching vibrations of phenolic C–OH groups that are typical of oil ester. The absorption signal observed at 736 cm^{-1} is probably due to bending of CH bonds. The band appearing at 1436 cm^{-1} could be observed due to bending vibrations of the alcohol C–OH group and bending vibrations of C=C and CH in the methylene group. The stretching of –CN bonds also generate the peak at 1353 cm^{-1} . The presence of PSO-NE in water is indicated by a significant peak at 3467 cm^{-1} , corresponding to the stretching vibrations of the O–H group. The signal at 1639 cm^{-1} denotes the stretching vibration of the C=O bond in an aldehyde. The peak at 1097 cm^{-1} is ascribed to the stretching of the C–O–C bond. The use of surfactant in the formulation may have enhanced peak sizes in PSO-NE spectra. The spectra of Tween 80 exhibit different peaks, encompassing the stretching of the OH functional group, C–H bonds in the methylene group, C=O bond stretching, C–O–C stretching, and CH bond bending³¹ (Fig. 4).

Physicochemical characterization

UV-spectroscopic observations at a wavelength of 600 nm serve as an indicator of the level of cloudiness or haziness in PSO-NE. There is an inverse relationship between the absorbance value and the concentration of surfactant. As the concentration of surfactant increased from 1:1 to 1:3, the turbidity decreased. The pH values exhibited a positive correlation with the surfactant concentration, as concentration of surfactant increased from 1:1 to 1:3, pH values also increased, as observed in Table 3 and Fig. 5.

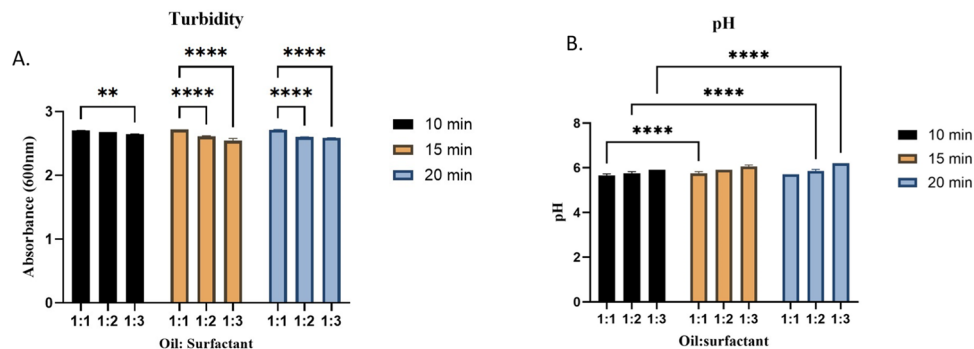


Fig. 5. (A) Characterization of the formulations involved the use of UV-spectroscopic measurement at a wavelength of 600 nm to determine the turbidity of the PSO-NE after being sonicated for 20 min. (B) The pH values of PSO-NE vary with surfactant concentration ranging from 1:1 to 1:3 after being sonicated for 20 min. Data are representative of three experiments expressed as mean \pm SD ($n = 3$). * $P < 0.05$, ** $P < 0.01$, *** $P < 0.001$ using one way ANOVA Tukey post test.

Formulation	Sonication time (min)	Centrifugation	Heating cooling cycle	Freeze–Thaw cycle	% Δd_z	% $\Delta \zeta_f$	Inference
A1	10	✓			13.6	-8.9	Failed
A2	10	✓			10.8	-8.8	Failed
A3	10	✓	✓		11.2	-9.1	Failed
B1	15	✓			8.5	-10.7	Failed
B2	15	✓	✓		7.7	-7.6	Failed
B3	15	✓	✓	✓	3.6	-1.2	Passed
C1	20	✓	✓		5.6	-1.0	Failed
C2	20	✓	✓	✓	2.3	-1.5	Passed
C3	20	✓	✓	✓	2.1	-0.6	Passed

Table 4. Analysis and deductions of PSO-NE stability investigations at different concentrations.

Stability

All the sonicated formulations did not undergo phase separation during the centrifugation test and were thus preceded towards further testing. Except B3, C2, and C3, all the sonicated formulation underwent phase separation and show major change in droplet size and zeta potential during heating–cooling cycles and freeze–thaw tests and was thus excluded from further testing as detailed in Table 4. The influence of stressors on the stability and efficacy of optimized PSO-NE (B3, C2, and C3) is presented in Table 4, which shows the d_z , and ζ_f values derived from measurements of nanoemulsion samples prior to exposure of stressor. Based on the % Δd_z data, and % $\Delta \zeta_f$ we deduce that heating–cooling cycles and freeze–thaw tests exert negligible effects on the nanoemulsion characteristics, other from a minor increase in droplet sizes. The best formulation was determined by considering the particle size and PDI value from a restricted selection of formulations. As previously stated, longer sonication periods result in increased stability (reduced droplet size) of a nanoemulsion. This narrows down the selection of ideal formulations to C2 and C3. The preceding section also presented data indicating that increased surfactant concentrations result in enhanced stability (reduced droplet size) and improved homogeneity (reduced polydispersity index). This led to the choice of C3 as the preferred formulation for further investigation in the research.

MTT assay

The cells were exposed to several concentrations of C3, PSO and Blank PSO-NE. It was observed that the PSO-NE effectively suppressed the proliferation of breast cancer cells at IC_{50} value of 46.6 $\mu\text{g/ml}$ and 60 $\mu\text{g/ml}$ for MCF-7 and MDA-MB-231, respectively. However, C3 did not exhibit any inhibitory effect on non-cancerous Vero cells (Fig. 6). Considering the cytotoxicity of PSO with respect to IC_{50} indicates that 200 $\mu\text{g/ml}$ and 350 $\mu\text{g/ml}$ of PSO is required to eradicate half population (50%) of MCF-7 and MDA-MB-231 cells, respectively. Blank PSO-NE did not show any inhibitory effect on MCF-7 and MDA-MB-231.

PSO-NE uptake study

A fluorescent lipophilic substance (Rhodamine-B) was added to the prepared nanoemulsion (Rho-PSO-NE) and with PSO (Rho-PSO) to ascertain the internalization of PSO-NE and PSO in breast cancer cells. After 4 h, as shown in Fig. 7, Rhod-PSO-NE was uniformly and effectively internalized throughout the cytoplasm of MCF-7 and MDA-MB-231 cells (Fig. 7). While, Rho-PSO did not show any internalization within the cells. Mean fluorescence intensity was calculated using confocal microscopy, shows uptake efficiency of PSO and PSO-NE

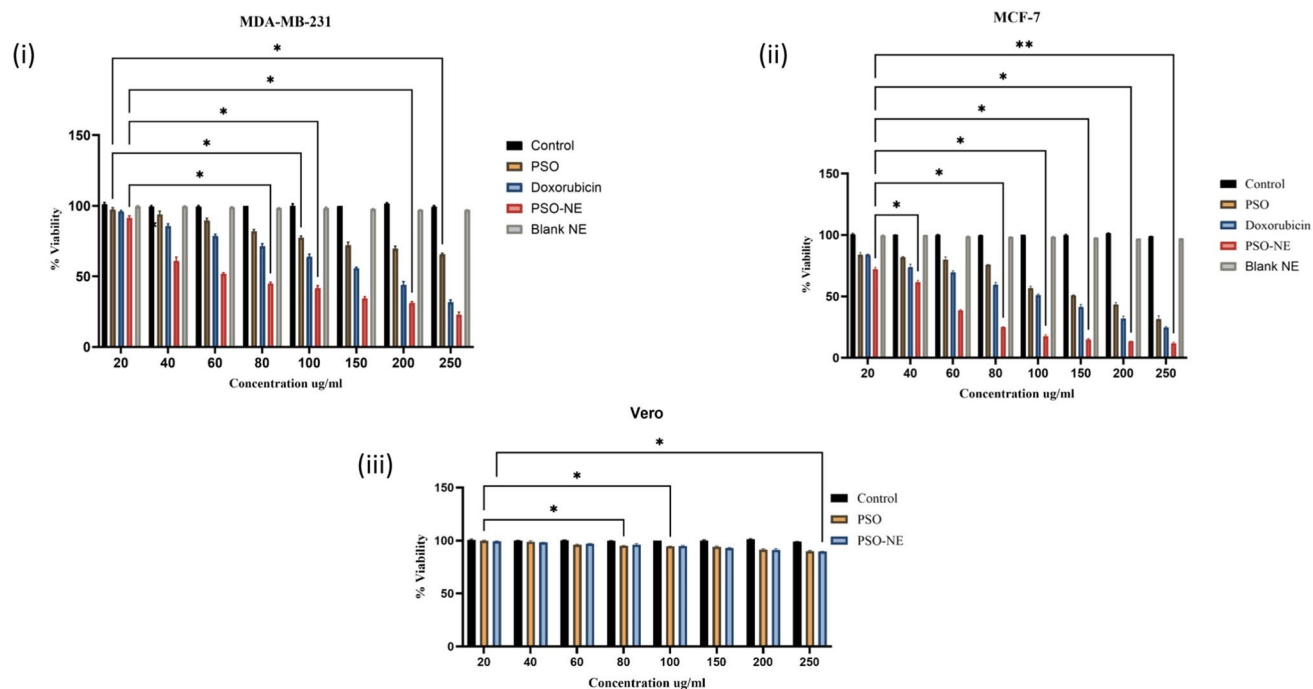


Fig. 6. Cytotoxicity fo PSO-NE on % viability of (i) MDA-MB-231 cells (ii) MCF-7 cells (iii) % viability of Vero cells treated with PSO, PSO-NE and Doxorubicin. The results are expressed as the mean \pm SD (n = 3). *P < 0.01 when compared with control using one way ANOVA Tukey post test.

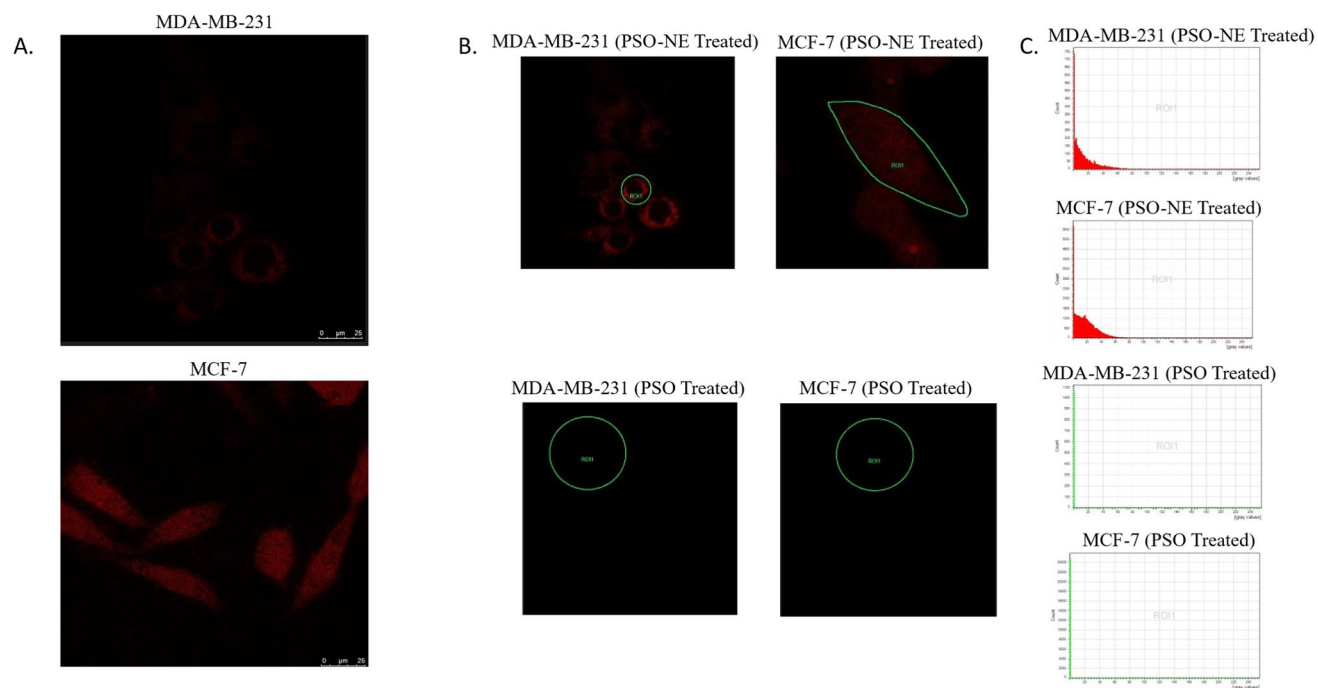


Fig. 7. (A) Confocal images showing uptake of rhodamine-B loaded PSO-NE by the cells. Scale bar = 25 μ m. (B) Confocal images showing ROI (Region of interest) in PSO-NE and PSO treated cells. (C) Mean Fluorescence intensity showing uptake efficiency in PSO-NE and PSO treated cells.

by cells. As compared to PSO treated cells, PSO-NE treated cells show higher uptake efficiency of 80% in MCF-7 and 75% in MDA-MB-231.

DAPI nuclear morphology assay

The DAPI nuclear staining showed the morphological changes between control and treated cells. The Fig. 8 showed that the cells treated with PSO-NE have condensed nuclear material in both the cell lines MCF-7 and MDA-MB-231. The condensed nuclear morphology depicts apoptotic changes in PSO-NE treated cells in comparison to smooth nuclei observed in control and PSO treated cells (Fig. 8).

Apoptosis analysis by Annexin-V FITC/PI

The PSO-NE treated cells exhibited a notable rise in the proportion of PI-Annexin-V FITC+ cells (indicating early apoptosis) and a reduction in PI-Annexin-V FITC cells (indicating viable cells) compared to the control cells. As compared to the PSO treated cells where, the proportion of cells in the early stages of apoptosis increased from 3.10 to 8.25% and from 0.33 to 4.19%, respectively in the treated MCF-7 and MDA MB231 cells, the proportion of cells in the early stages of apoptosis increased from 3.10 to 21.5% and from 0.33 to 14.6%, respectively, in the PSO-NE treated MCF-7 and MDA MB231 cells as observed in Fig. 9.

CFSE cell proliferation assay

The CFSE fluorescent dye was employed to confirm the findings of the MTT assay in the cell proliferation assay. Figure 10 illustrates the proliferation pattern of the PSO-NE labeled with CFSE in the treated cells (MCF-7 and MDA MB-231) compared to the control and PSO treated cells. The cell growth rate was reduced from 99.2% and 74.59% in control and PSO treated cells, respectively to 54.4% in PSO-NE treated MCF-7 cells and from 99.3% and 80.54% in control and PSO treated cells, respectively to 55.2% in PSO-NE treated MDA MB-231 cells, as observed in Fig. 10.

Cell cycle arrest analysis

The assay results demonstrated that the percentage of cells in the G0/G1 phase increased from 50.7% in control cells to 71.9% in treated cells of MCF-7. Conversely, the percentage of cells in the G2/M and S phases decreased from 37.8 and 36.0% in control cells to 22.4% and 12.5% in treated cells of MCF-7. The percentage of cells in the G0/G1 phase increased from 41.5% in control cells to 68.9% in the treated cells of MDA MB-231. Conversely, the percentage of cells in the G2/M and S phase decreased from 26.3% and 34.8% in control cells to 10.8% and 28.0% in treated cells of MDA MB-231, respectively (Fig. 11). The findings from the cell cycle study indicate that both cell lines (MCF-7 and MDA MB-231) experienced cell cycle arrest in the G0/G1 phase. In PSO treated MCF-7 cells G0/G1 phase increased to 62.8%, S and G2/M phase increased to 35.5% and 28.6%, respectively. Furthermore, in PSO treated MDA-MB-231 cells G0/G1 phase increased to 53.7%, S and G2/M phase increased to 30.6% and 22.5%, respectively.

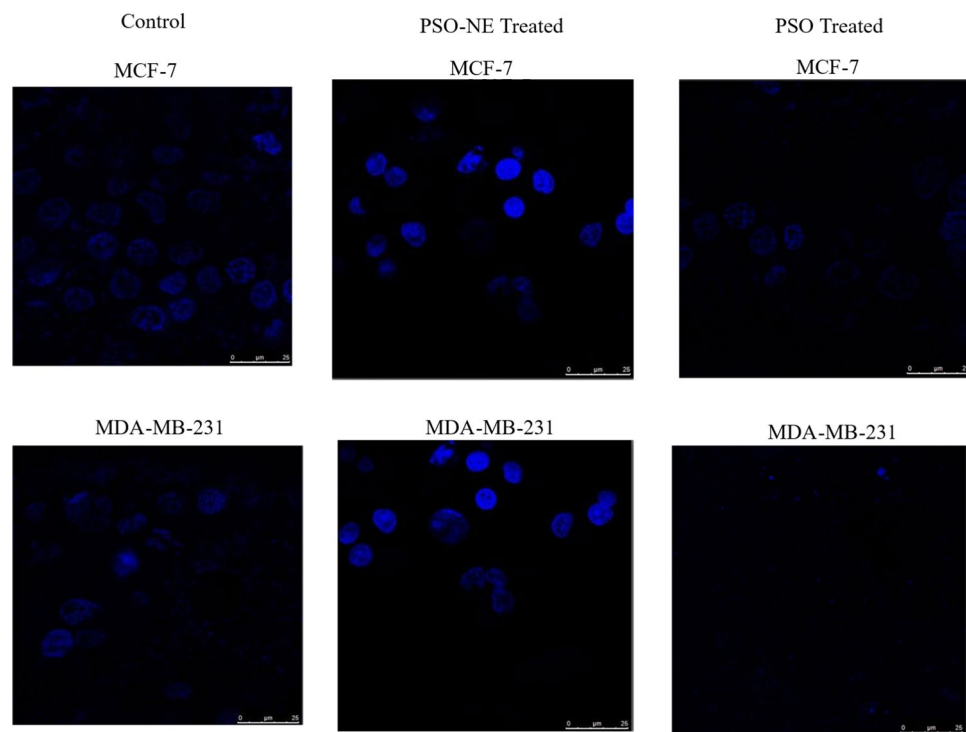


Fig. 8. Confocal images of DAPI nuclear staining (scale bar for MCF-7 = 25 μ m and for MDA MB-231 = 25 μ m).

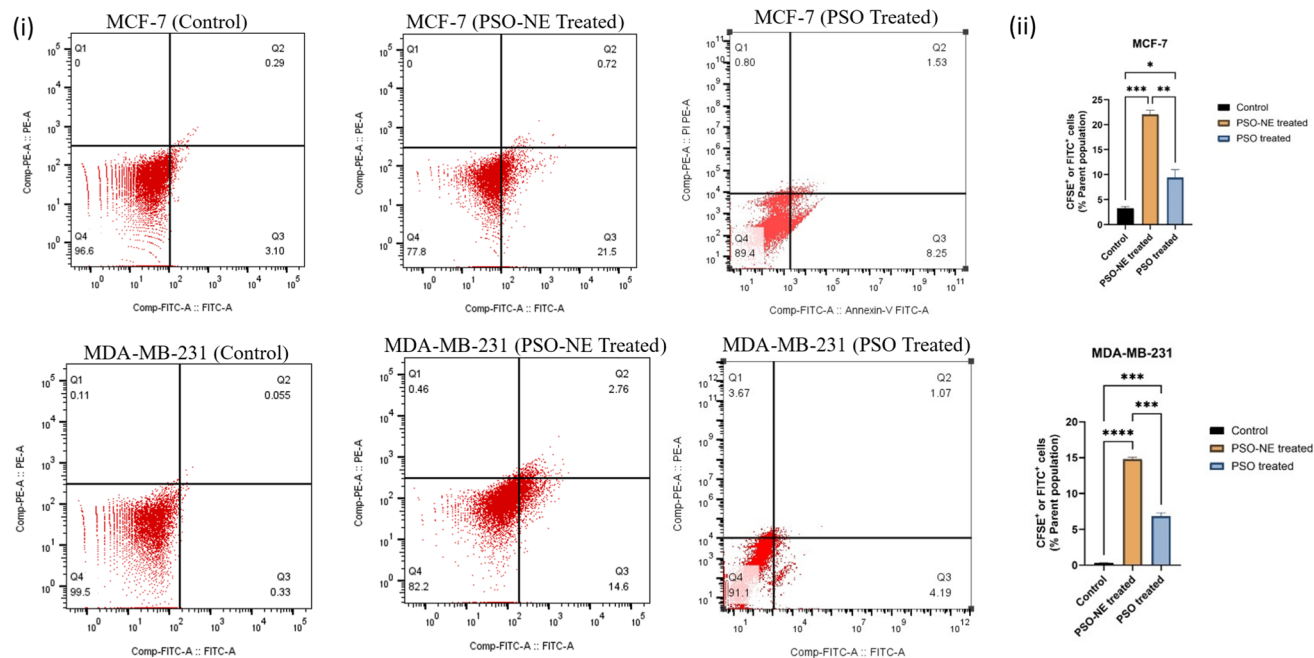


Fig. 9. Apoptosis assay (i) Plot and Graph denoting annexin V/PI staining used to monitor cells (FITC + PI +) are shown in Q3 and Q2 quadrant, respectively (ii) The percentage of early apoptotic cells. Data are representative of three experiments expressed as mean \pm SD (n = 3). *P < 0.05, **P < 0.01, ***P < 0.001 when PSO-NE treated cells compared with control cells using unpaired t-test.

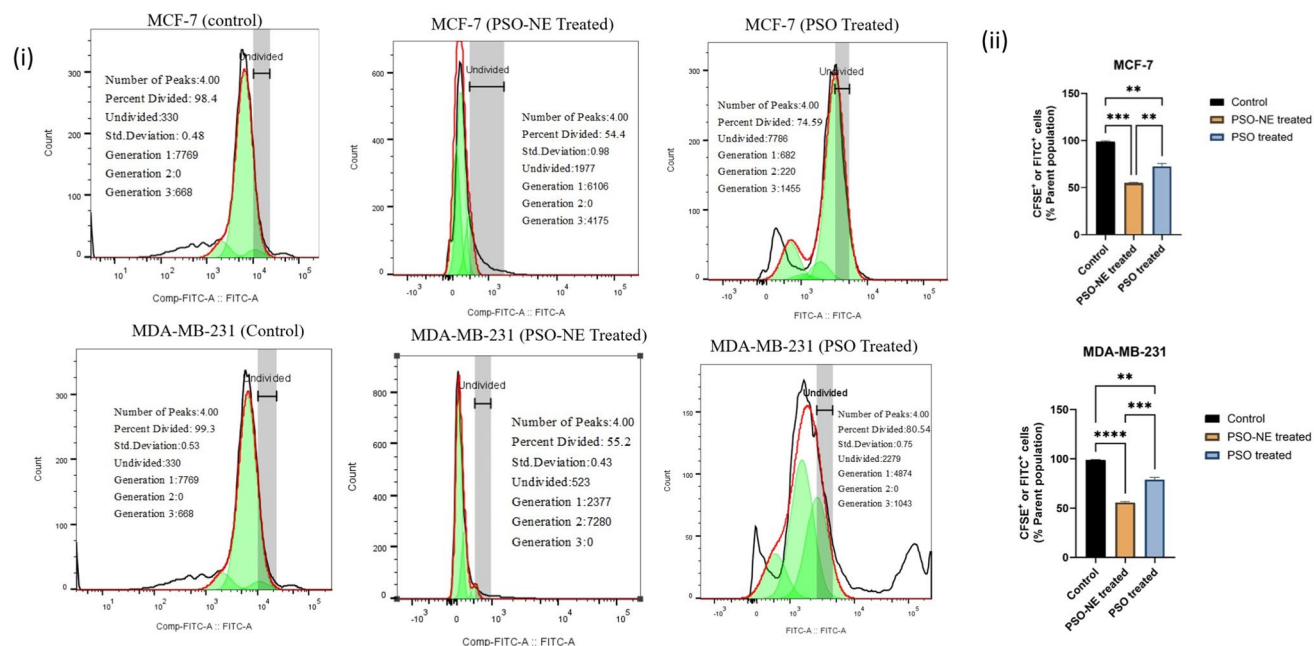


Fig. 10. CFSE cell proliferation assay (i) Plots and (ii) Graph showing the percentage of viable cells. Data are representative of three experiments expressed as mean \pm SD (n = 3). *P < 0.05, **P < 0.01, ***P < 0.001 when PSO-NE treated cells compared with control cells using unpaired t-test.

Real-time PCR analysis

In the real-time PCR analysis of the both MCF-7 and MDA-MB-231 cell lines the expressions of genes (Bcl-2, STAT-3 and NF- κ B) correspond to proteins related to the cell proliferation was significantly down regulated and genes (p53, Bax and caspase 3) correspond to the proteins related to apoptosis were significantly up-regulated compare to the untreated and PSO treated cell lines, as detailed in Fig. 12.

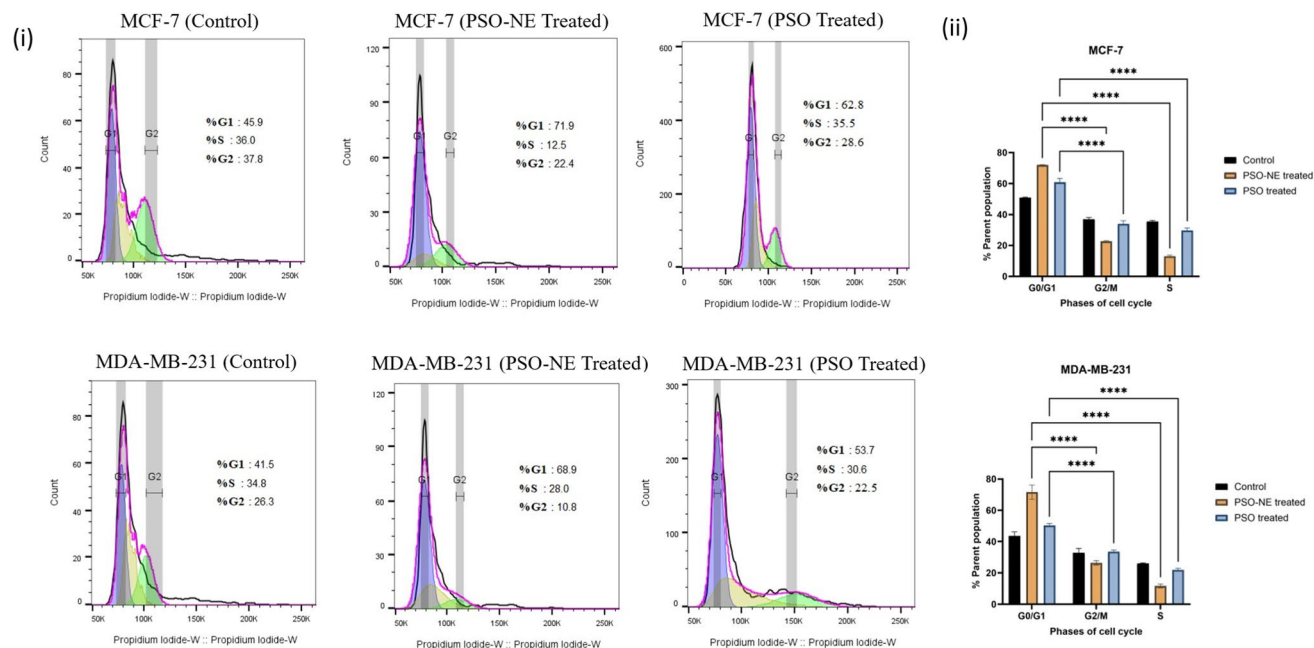


Fig. 11. Cell cycle study by propidium iodide (PI) (i) Plots and (ii) Graph depicting percentage for cells in G0/G1, G2/M and S phase. The values are represented as the mean \pm SD (n = 3). *P < 0.01, **P < 0.01, ***P < 0.001 when PSO-NE treated cells compared with control cells using unpaired t-test.

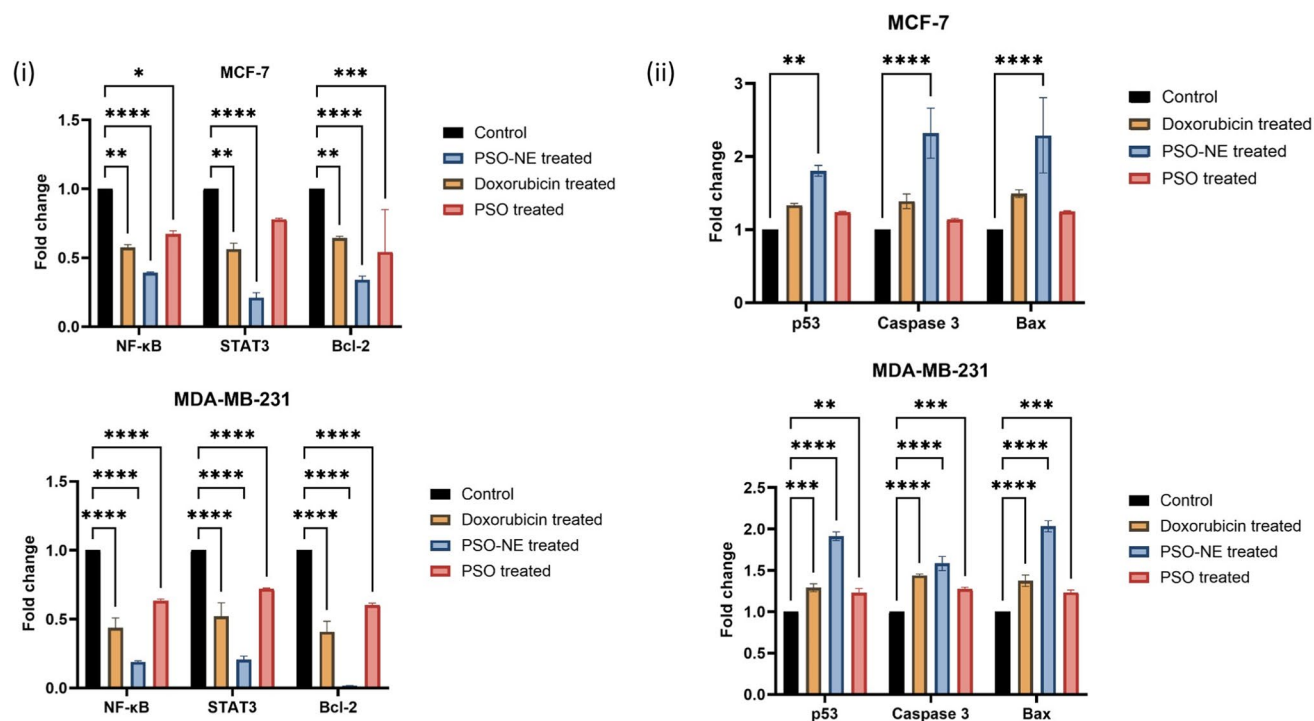


Fig. 12. Real-time expression of the significantly highly differentially expressed genes corresponds to the protein related to (i) proliferation (ii) apoptosis. The results are expressed as mean \pm SD (n = 3). *P < 0.01, **P < 0.01, ***P < 0.001 when PSO-NE treated group compared with control group using one way ANOVA Tukey post test.

Discussion

Gas chromatography has shown to be the most suitable method for separating and analyzing the several components in oils³². In this study, GC–MS analysis of PSO identified 19 active compounds. PSO contained a prominent amount of Octadecadienoic acid (z,z)- (37.41%), Hexadecanoic acid, methyl ester (28.28%), Methyl stearate (14.41%), 9-Octadecenoic acid, methyl ester, (e)- (6.10%), Squalene (2.68%), and Hexadecadienoic acid, methyl ester (2.13%). The compound 9, 12-octadecadienoic acid, methyl ester (Z, Z) has been shown to have potent anticancer activity against the A549 human lung cancer cell line. 9, 12-octadecadienoic acid, methyl ester (Z, Z) is a dually unsaturated fatty acid, commonly found in plant glycosides. It is a crucial fatty acid in the diet of mammals and is involved in the production of prostaglandins and cell membranes³³. Octadecanoic acid is the main metabolite found in plants, and combines with glycerol to generate esters. Studies have demonstrated that octadecanoic acid exhibits anticancer properties in mice models and specifically targets MOLT-4 in leukemia cancer cells by interacting with DNA topoisomerase I and inducing death in tumor cells³⁴. Furthermore, hexadecanoic acid methyl ester possesses antioxidant, nematocidal, insecticidal, anti-inflammatory, and antiandrogenic characteristics³⁵. In addition, stearic acid (stearate) is found in large quantities in the dietary foods and has several biological effects, such as Stearate has been demonstrated to suppress the proliferation of Hs578t breast cancer cells mediated via the epidermal growth factor (EGF) receptor³⁶, prevent the invasion of HT-1080 fibrosarcoma cells³⁷, and trigger the apoptosis in MDA-MB-231 breast cancer cells³⁸. Furthermore, cytotoxic action was shown in squalene extracted from algae against leukemia (Jurkat), sarcoma (CADO-ES-1), cervical cancer (HeLa), and multiple carcinoma (MM1440). In addition to their inhibitory function, squalene compounds also possess the capacity to induce apoptosis in several neoplastic cell lines, including leukemia, melanoma, colon cancer, prostate cancer, ovarian carcinoma, liver cancer, breast cancer, lung cancer, and peripheral nerve system carcinoma³⁹. This indicates that the active compounds in PSO exhibit diverse cytotoxic properties.

We have effectively synthesized PSO-NE using PSO, Tween 80 and MilliQ water through high-energy ultrasonication method. Several studies have reported formulation of PSO-NE through different methods such as, self-emulsifying method, phase inversion temperature (PIT) method, homogenization, and pseudo-ternary phase diagrams^{26–28,40}. High-energy ultrasonication method surpasses for operational efficiency and cleanliness. Strong disruptive forces from high ultrasound energy are utilized to split apart big droplets into nanoparticles and create high-kinetic-energy nanoemulsions. By utilizing ultrasonication techniques, we may select the formulation composition and achieve more control over particle size. Moreover, it provides regulation over the emulsion's color, rheology, and stability⁴¹. The surfactant has a crucial role in stabilizing and regulating the size of droplets, which is essential for formulating nanoemulsions⁴². The production of PSO-NE is non-spontaneous since the Gibbs free energy involved in the process is positive. The surfactant greatly decreases the amount of free energy required in the process of nanoemulsion formulation⁴³. Tween 80 was used for this study due to its propensity to promote the creation of oil-in-water NE as shown in Fig. 13. This surfactant is widely recognized for its ability to quickly adhere to the surface of droplets. It has a relatively low molecular weight, is nonionic, and has a hydrophilic-lipophilic balance (HLB) ratio of 15. It functions as a potent agent in decreasing the size of droplet diameter in comparison to other ionic surfactants like CTAB and SDS⁴⁴. Tween 80 is classified as Generally Recognised As Safe (GRAS) for application in medicines and as a food surfactant⁹. Pavoni et al.⁴⁵ had demonstrated that out of all the surfactants evaluated, Tween 80 emerges as the superior option, as it facilitated the attainment of an ideal oil in water nanoemulsion regarding droplet size and PDI, while simultaneously ensuring prolonged stability of the system. Furthermore, favorable outcomes were attained about the cytotoxicity of Tween 80, which emerged as the safest surfactant (highest LC50) among all those evaluated.

The process of ultrasonic emulsification results in the formation of microscopic droplets that have a low polydispersity index, as seen in Table 2. The polydispersity index serves as a quantitative indicator of the uniformity and stability of the nanoemulsions⁴⁶. In this study, the application of ultrasonic technology resulted in the creation of a PSO-NE with a PDI value of 0.189, indicating the successful fabrication of a stable PSO-NE

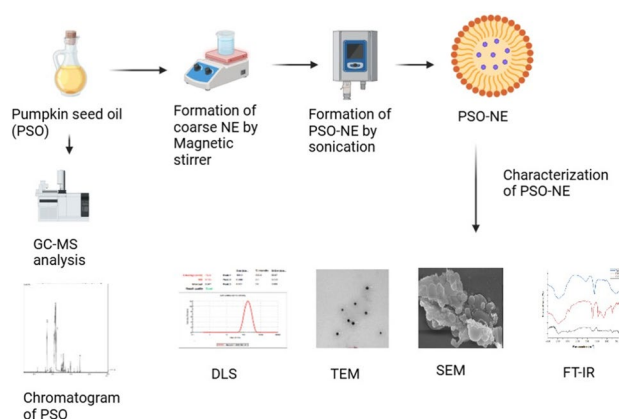


Fig. 13. Formulation of Pumpkin seed oil nanoemulsion (PSO-NE) by ultrasonication method. Tween 80 was used as a surfactant.

with evenly dispersed particle sizes. Periasamy et al.⁹ previously reported PDI of 0.117 of formulated *N. sativa* essential oil nanoemulsion (NSEO-NE).

The zeta potential serves as a fundamental factor influencing the stability of a nanoemulsion. The observed negative zeta potential in PSO-NE arise from the adsorption of negative ions onto the surface of oil droplets, as well as from the presence of functional groups within the chemical constituents of PSO, including hydroxyl groups (–OH) and carboxyl (C=O) groups^{47,48}. The observed reduction in zeta potential (from –34.5 to –24.3 mV) with increasing surfactant concentration may initially seem inconsistent with the assertions of stability. Colloidal stability is influenced by both electrostatic and steric processes, especially in systems containing surfactants. The reduction in zeta potential indicates less electrostatic repulsion, whereas the adsorbed surfactant layers presumably provide steric stabilization, which prevails at elevated concentrations⁴⁹. Ghosh et al.⁵⁰ and Zirak and Pezeshki⁵¹ had reported that systems can maintain stability at moderate zeta potentials (e.g., $|\zeta| > 20$ mV) provided steric hindrance from surfactant chains surpasses electrostatic weakening.

The minute droplets generated using ultrasonication method possesses a significant surface area, facilitating the effortless penetration of active substances into blood arteries¹⁹. Longer sonication times would result in higher net input energy, greater disruption of droplets, and further reduction of droplet size⁵². This pattern also aligned with our study's findings. By increasing the sonication period (10–20 min) and surfactant concentration (1:1–1:3), DLS measurements of droplet size and polydispersity index showed a significant decrease. However, any increase over a 20-min sonication period and a 1:3 oil-surfactant ratio proved ineffectual. Consequently, it was found that C3 was the best formulation for further characterization. Our findings align with a previous study of Periasamy et al.⁹ that there is reduction in droplet size with increased surfactant content.

In addition to assessing the physical stability of the formulations, measurements of turbidity and pH were conducted. These factors are crucial in determining the effectiveness of the PSO-NE in delivering drugs. The research suggests that the reduction in absorbance is likely due to the comparatively mild scattering from translucent emulsions⁵³. The higher turbidity observed in all PSO-NE formulation is likely due to the nature of pumpkin seed oil, which can increase mild scattering. As pumpkin seed oil is a carrier oil so as comparable to other nanoemulsion which is mainly formulated with essential oil has more turbidity. Carrier oil contains more polyunsaturated fatty acids than essential oil⁵⁴. Lozada et al.¹⁶ had demonstrated that the pumpkin seed oil nanoemulsions prepared were translucent, or milky appearance and cloudy in appearance. Using pH and viscosity to characterize a nanoemulsion can help with rheological investigations and the development of medication delivery strategies for *in-vivo* use.

The morphological examination of PSO-NE was conducted using TEM. The PSO-NE has a dark and spherical shape, with a diameter ranging from 50 to 150 ± 0.27 nm (Fig. 6), which is consistent with the particle size determined by DLS. The PSO-NE exhibited a homogeneous shell droplet without any formations of aggregations or coalescence. The stabilizing action of Tween 80 can be ascribed to its high mobility, since it forms a protective layer around the particles of PSO, preventing them from clustering together⁵⁵. SEM images revealed the presence of minor aggregation, a characteristic frequently observed in emulsion systems during SEM analysis. This aggregation can be attributed to the sample dehydration procedure preceded the analysis⁵⁶. Nevertheless, particle diameters in SEM images and those determined by DLS, correlated well. Alam et al.⁵⁷ illustrate similar morphological study of ultrasonic nanoemulsion of *Cinnamomum cassia* L. essential oil through TEM and SEM analysis.

For identifying potential interactions between PSO and surfactant utilized in a formulation, Fourier Transform Infrared Spectroscopy (FT-IR) is an indispensable analytical instrument. Peaks of PSO-NE was identical to those detected in PSO, except for the first peak noted in the nanoemulsion at 3467 cm^{–1}, which corresponds to H-OH stretching, suggesting the presence of water in the emulsion. The additional significant peaks at 1743.53 cm^{–1} and 1640.96 cm^{–1}, associated with the C=O stretch, signify the existence of esters in the oil, consistent with the spectra of PSO. The absence of additional peaks, aside from the H-OH bond peak, confirms that no chemical alterations occurred during emulsification via ultrasonication⁵⁸. However, no other peak was seen, indicating that PSO was chemically stable and only confined inside nanoemulsion. Our findings are aligning with the earlier findings of Perumal et al.³¹. The use of surfactant in the formulation may have resulted in the enlargement of peaks in the PSO-NE spectra⁵⁹.

Stress-testing was conducted to assess its colloidal stability against various environmental variables. These approaches replicate several stress conditions, including gravity separation, temperature variations, and freeze-induced destabilization that may arise during packaging, shipping, or handling. Evaluating the formulation under these conditions aids in forecasting its durability and resilience to instability mechanisms, including creaming, coalescence, and phase separation⁶⁰. The optimized PSO-NE (C3) exhibited significant thermodynamic stability under all evaluated conditions. The results emphasize the formulation's capacity to withstand diverse stressful circumstances, rendering it appropriate for practical applications in which stability amid varying temperatures and physical stress is essential. Srilatha et al.⁶¹ conducted thermodynamic investigations on glipizide nanoemulsion, subjecting it to three stability cycles, and showed favorable physical stability with no evidence of phase separation, creaming, or cracking. Azeem et al.⁶² and Al-Balushi et al.⁶³ have illustrated that the thermodynamic stability provides the nanoemulsion with a longer lifespan. Thus, the results validate that the PSO-NE (C3) are effectively designed for short- and long-term storage. Nevertheless, accelerated long term stability studies of PSO-NE have not performed and thus the future studies will incorporate accelerated stability testing to deliver a more thorough assessment of long-term stability.

The PSO-NE exhibited a concentration-dependent cytotoxicity profile. The PSO-NE shown superior efficacy in inhibiting the growth of MCF-7 and MDA-MB-231 cells compared to free PSO and doxorubicin. Furthermore, blank NE did not exhibit inhibitory effect on breast cancer cells suggesting that the observed effects are attributable to PSO and not the delivery system. Nayila et al.⁶⁴ and Periasamy et al.⁹ had reported similar results that 2-carene nanoemulsion and *Nigella sativa* L. essential oil nanoemulsion enhances the

bioavailability of respective oil on breast cancer cells. The primary drawback of chemotherapeutic agents is their lack of selectivity, resulting in harmful effects on healthy tissues⁶⁵. Consequently, in the present study, the cytotoxicity of PSO-NE was assessed against normal Vero cells to evaluate their safety. PSO-NE did not exhibit any inhibitory effect on non-cancerous Vero cell lines.

It has been found that nanoemulsions (100–200 nm and \approx 30 mV) are preferentially taken up by cells through the endosomal pathway^{66,67}. Similarly, in our findings, Rhod-PSO-NE was uniformly and effectively internalized throughout the cytoplasm of MCF-7 and MDA-MB-231 cells and show higher uptake efficiency as compared to free PSO suggesting emulsification enhance the bioavailability of oil.

One efficient strategy employed by cytotoxic drugs is the induction of apoptosis and cell cycle arrest to inhibit cell growth⁶⁸. The program cell death pathway induced by PSO-NE was analyzed using Annexin-V FITC/PI, focusing on two mechanisms: apoptosis and necrosis⁶⁹. It has been reported by Nirmala et al.⁵² that celery nanoemulsion had induces early apoptosis in SAS cells. Similarly, Abd-Rabou and Edris⁶⁵ also demonstrated induction of early apoptosis in A549 cell line when treated with Frankincense essential oil nanoemulsion. Our investigation verified that when breast cancer cells (MCF-7 and MDA-MB-231) treated with PSO-NE, the early apoptosis has induced in majority of the cells (Annexin V + /PI –) compared to PSO treated cells.

Our study demonstrated that PSO-NE can effectively arrest the progression of cell lines in the G0/G1 phase of the cell cycle and induce programmed cell death in the treated cancer cells. Our results have differed from Salehi et al.⁶⁸ who reported cell cycle arrest at G2/M phase in MCF-7 and MDA-MB-231 cells when treated with apple pectin-based *Zataria multiflora* essential oil (ZEO) nanoemulsion. This variation can likely be attributed to DNA fragmentation resulting in morphological alterations associated with apoptosis and necrosis. However, in our study, a direct mechanistic correlation to specific components of pumpkin seed oil (PSO) was not established. PSO contain many bioactive compounds such as phytosterols, tocopherols, and unsaturated fatty acids, many of which have been reported to inhibit cell proliferation and induces cell cycle arrest. For instance, β -sitosterol significantly arrest cell cycle at G0/G1 phase in breast cancer cells⁷⁰, and tocopherols induces modulation of cyclin expression⁷¹.

The population of cells is exposed to carboxyfluorescein diacetate succinimidyl ester (CFDA-SE), which is a membrane-permeable form of CFSE. Once CFDA-SE has permeated the cell membrane, cellular esterase catalysis the break down the acetate groups leads to the formation of CFSE, which is both extremely fluorescent and impermeable. When CFSE is added at appropriate quantities and the pH is neutral, it does not have any negative impact on the cell's function. During cell division, the CFSE fluorescence intensity (FI) is distributed almost equally across the two resulting daughter cells⁷². Hence, the quantification of FI serves as an indirect assessment of the cellular divisions. In Our study, FI reduced in PSO-NE treated cells as comparable to PSO treated and control cells, indicating decrease in cell proliferation upon treated with PSO-NE.

DAPI can readily penetrate intact cell membranes and ultimately attaches itself to the minor groove of DNA sections that are rich in A-T base pairs. DAPI is a nuclear morphology indicator that is commonly used to differentiate apoptotic cells based on the size and roundness of the nucleus⁷³. In our study, the condensed nuclear morphology depicts apoptotic changes in PSO-NE treated cells in comparison to smooth nuclei observed in control and PSO treated cells. Similar results had reported by Alkhatib et al.⁷⁴.

The current study evaluated genetic expressions of pro-apoptotic markers (Caspase 3 (Cas3), p53, and Bax) together with anti-apoptotic markers (Bcl-2, NF- κ B, and STAT-3) to substantiate the findings from the apoptosis and cell cycle assay. p53 activation protects normal cells from chemotherapy-induced cytotoxicity by modifying cell cycle checkpoints, specifically during the S-phase or M-phase^{75,76}. This idea opened a therapeutic window for the creation of new anti-cancer drugs, like PSO-NE in this study that can increase the expression of the p53 gene. This induces apoptosis in cancer cells while simultaneously maintaining the health of normal cells by regulating their cell cycle checkpoints. In the internal pathway of apoptotic, activated caspase-8 necessitates mitochondrial involvement involving the Bax and Bcl-2 genes. Bax is up-regulated by active caspase-8 and relocated to the mitochondria. This changes mitochondrial membrane polarization and releases cytochrome c to generate an apoptosome⁷⁷. The apoptosome plays a crucial role in the activation of various caspases, specifically caspases 9, 3, 6, and 7⁷⁶. In breast cancer cells, PSO-NE up-regulate Bax and caspase 3 and down-regulate Bcl-2 genetic expression relative to PSO treated and control cells which is align with the findings of Abd-Rabou and Edris⁶⁵. The emergence of chemoresistance is a recognized phenomenon that can occur during cancer therapy. This results in cancer recurrence due to the activation of certain survival (anti-apoptotic) genes, including NF- κ B and STAT-3⁶⁵. Consequently, the suppression of these genes represents a compelling therapeutic approach, which is incorporated in the present investigation. NF- κ B and STAT3 genes were down-regulated in breast cancer cells upon treatment with PSO-NE formulation.

The results of this study demonstrated, for the first time, the potential of a PSO-NE to exhibit anticancer activity against breast cancer cells in *in-vitro* experiments. The formulation therefore has strong anticancer potential.

Methods

Reagents

For this study, we purchased the Indian-origin *Cucurbita maxima* (Pumpkin) seed oil from Cyrus Enterprises in Chennai, India. Cold press method was employed in extracting oil as per the manufacturer's datasheet. We obtained the non-ionic surfactant polyoxyethylene sorbitan monooleate (Tween 80) from Merck, India. MTT, DAPI, propidium iodine, RNase, and rhodamine were acquired from HiMedia Laboratories, India. The Annexin V-FITC Early Apoptosis Detection Kit was obtained from eLabScience, India. We obtained the CFSE proliferation kit, Verso cDNA kit, SYBR Green real-time PCR master mix and DNase I from ThermoFisher Scientific-Life science Solution, India. The Carbunn RNA Purification kit was obtained by JITM C Genes, UP, India. The water used for all the procedure was double-distilled in a Milli-Q system (Millipore Corporation).

Gas chromatography–mass spectrometry (GC–MS) analysis

Production of fatty acid methyl esters (FAME)

The conversion of fatty acids into their derivatives, such as fatty acid methyl esters (FAME), is integral to the process of GC–MS analysis. The procedure entails, as per Uba and Muhammad⁷⁸, the addition of 1 g of extracted oil and 2% methanolic KOH to a 50 ml round bottom flask, followed by heating in a water bath for 1 h, cooling to room temperature, adding 40 ml of n-hexane, and subsequently separating the organic layer. The esterified sample is subsequently concentrated using rotary evaporation.

GC–MS analysis

To analyze the active components and their chemical structure in pumpkin seed oil; GC–MS was conducted using a Shimadzu GC-MS-QP 2010 instrument. The instrument used in this study was facilitated with an auto-injector and a mass selective detector. The ion source temperature was set at 220 °C, the interface temperature was at 270 °C, the solvent cut time was 3.50 min, the threshold was 1,000 eV, and the mass range was 40 to 650 m/z. An Rxi-5 Sil MS capillary column (30 m long, 0.25 mm wide, and 0.25 mm thick) made by Restek Company in Bellefonte, United States, was used to separate the parts. The investigation employed parted delivery technique with a split proportion of 10:1 and the thermostat set at 260 °C, with seed oil injection volume of 1.0 L. The oven temperature was raised to 300 °C at 10 °C per minute for 16 min, with helium as the carrier gas. The total flow and column flow remained at 16.3 and 1.21 ml/min, respectively, for compound identification. A determination of elements was carried out through a comparison of their compared accumulation time and mass distribution with entries in the National Institute of Standards and Technology (NIST) database and the WILEY8 spectrum library.

Formulation of pumpkin seed oil nanoemulsion

Preparation of pumpkin seed oil nanoemulsion (PSO-NE) consists of pumpkin seed oil, Tween 80, and MilliQ water. In this study, PSO-NE formulation was a twofold process, where the first step was formulation of coarse emulsion by mixing MilliQ water at a speed of 500 rpm while stirring to the organic phase composed of varying oil: surfactant (1:1, 1:2, and 1:3) concentrations. The oil content in all the combinations was consistently maintained at a fixed concentration of 6%. Subsequently, the coarse emulsions were transformed into their corresponding nanoemulsions at 50% amplitude by using 750W ultrasonicator (Biolink N Series Ultrasonic Probe Sonicator BL92-IINA). Each concentration underwent sonication for varying durations of 10, 15, and 20 min, respectively. A powerful and destructive force, caused by cavitation, is generated by supplying energy through a sonode with a probe diameter of 13 mm. This force can decrease the size of NE. The specimen vessel was positioned within a beaker filled with ice to counteract the thermal energy generated by sonication. The studies were conducted at room temperature. The prepared PSO-NE was stored at 4 °C.

Characterization of PSO-NE

Dynamic light scattering (DLS)

Formulated PSO-NE was characterized for an average size distribution (Z-average), polydispersity index (PDI) and Zeta potential by Zeta Sizer Ver. 7.12 (Malvern instrument) at 25 °C. Before the experiment, the samples were diluted with MilliQ water to a concentration of 100% in order to minimize the impact of multiple scattering effects. The measurement involved directing a laser beam with a wavelength of 633 nm through a 2 ml aqueous solution, with a detection angle of 90 degrees. The polydispersity index, Z-average, Zeta potential was computed, and a size distribution by intensity graph was produced. The DLS measurements were carried out in triplicate with mean S.D calculated.

Transmission electron microscopy (TEM)

The research employed TEM imaging at the Sophisticated Analytical Instrumentation Facility (SAIF) at the All India Institute of Medical Sciences (AIIMS), New Delhi, India, to examine the surface morphology of the PSO-NE, including size, structure, homogeneity, and roughness. The specimen was positioned on a carbon grid and thereafter immersed in 2% phosphotungstic acid (PTA) for duration of 2 min. The grid was dehydrated and examined using transmission electron microscopy. The image acquisition was performed using a Tecnai G2, 20 S-twin, FEI Electron Optics system, which features digital photography capabilities and a 35-mm visual equipment. Results were documented using a high-resolution digital CCD camera and analyzed via iTEM software.

Scanning electron microscopy (SEM)

Scanning electron microscopy (SEM) is used to examine the shape and structure of PSO-NE at different magnifications at the Sophisticated Analytical Instrumentation Facility (SAIF) at the All India Institute of Medical Science (AIIMS), New Delhi, India. The samples were prepared by drop-coating the formulation on a glass slide, dried, and analyzed using a high-resolution field emission scanning electron microscope. After striking with an electron beam, the samples produced secondary electrons, backscattered electrons, and specific X-rays. The SEM images were taken using a high-pressure technique at 20 kV with a working distance of 5000 ×.

Fourier-transform infrared spectroscopy (FT-IR)

The pumpkin seed oil, Tween 80 and formulated PSO-NEs were subjected to FT-IR analysis using Varian 7000 FTIR and Varian 600UMA FT-IR microscopes. The samples were gathered on a KBr pellet before being processed using the FT-IR spectrophotometer. The samples were analyzed by scanning them at wave numbers ranging from 4,000 to 400 cm⁻¹. The scanning was done with a resolution of 2 cm⁻¹ and 16 scans were performed for each sample. The data were analyzed using the Origin 2021b software.

Physicochemical characterization

Measuring the absorbance of the PSO-NE provides information on its turbidity and allows for quantitative confirmation of optically transparent solutions with varying oil-to-surfactant ratios. The absorbance of the undiluted PSO-NE is studied at 600 nm recorded by the UV-visible spectrophotometer (Hitachi). The measurements were carried out in triplicate with mean S.D calculated.

Determining the pH value is an indication of the stability of the PSO-NE. If any alterations in the pH are detected, they may be attributed to chemical processes⁷⁹. The pH of the undiluted formulations was measured using a Digital pH meter (EUTECH Instruments, Oakton, Singapore) at a temperature of 25 °C. The measurements were carried out in triplicate with mean S.D calculated.

Stability study

The stability of the produced PSO-NE, under high stress circumstances, was assessed by subjecting them to a centrifuge process (REMI International, India) at a speed of 3500 rpm for duration of 30 min. To assess the thermal stability of the created formulations that passed the previous test, the formulations underwent two types of cycles: a heating-cooling cycle and a freeze-thaw cycle. Initially, the heating-cooling process was performed three times by submitting the formulations to temperatures of 45 °C and 4 °C for duration of 48 h each. Subsequently, the freeze-thaw process was conducted at temperatures of – 20 °C and 25 °C, each lasting for 48 h, and this procedure was done thrice.

To quantify stress-induced instability in nanoemulsions, we computed the percentage change in droplet sizes (d_z) as follows:

$$\% \Delta d_z = \left(\frac{d_{z,f} - d_{z,i}}{d_{z,i}} \right) \times 100$$

where $d_{z,f}$ represents the z-average droplet size of the nanoemulsion following the application of the stressor, and $d_{z,i}$ denotes the initial value of d_z .

The equivalent quantity for fluctuations in ζ potential values is delineated as follows:

$$\% \Delta \zeta = \left(\frac{\zeta_f - \zeta_i}{\zeta_i} \right) \times 100$$

where ζ_f represents the zeta potential of the nanoemulsion after the application of the stressor, and ζ_i denotes the initial value. In this study, negative values of $\% \Delta \zeta$ signify destabilization due to a movement in the ζ potential value towards zero from either direction.

Cytotoxic activity

Cell culture

The breast cancer cell lines MCF-7 and MDA-MB-231 and non-cancerous Vero cell lines were procured from NCCS, Pune, India. The cells were cultured in DMEM media (HiMedia, Mumbai, India) containing 10% FBS (Fetal Bovine Serum, HiMedia, Mumbai, India) and supplemented with antibiotics (penicillin and streptomycin) (100X, HiMedia, Mumbai, India) at a temperature of 37 °C, with an atmosphere of 95% air and 5% CO₂.

MTT assay to determine the IC₅₀ value

MTT (3-(4, 5-Dimethyl-2-thiazolyl)-2, 5-diphenyl-2H-tetrazolium bromide) assay was performed to study the cytotoxic efficacy of the PSO, formulated PSO-NE, blank PSO-NE, and the control drug Doxorubicin on MCF-7 and MDA-MB-231 cells. The cytotoxicity of the PSO-NE was also examined against non-cancerous Vero cell lines. The cells were seeded on the 96 well culture plates at a density 1×10^4 cells/well and incubate for 24 h. Subsequently, the cells were exposed to PSO, Doxorubicin and PSO-NE, each at varying doses (20, 40, 60, 80, 100, 150, 200, 250 µg/ml). The cells were thereafter incubated for a period of 24 h. Following this, the solution of MTT was added to each well at a volume of 10 µl (5 mg/ml in PBS). The plates were subsequently subjected to an incubation period extending for an additional 4 h. Subsequently, the MTT was extracted, and the resultant formazan crystals were dissolved in 100 µl of DMSO, followed by gentle agitation. The absorbance was recorded at a wavelength of 570 nm utilizing the microplate reader (Spectra Max 340 PC, Molecular Devices, USA). The studies were conducted three times and the findings were reported as the percentage of viable cells in relation to the drugs being evaluated. The IC₅₀ values were determined by graphing the percentages of cell viabilities for MCF-7 and MDA-MB-231 cells against the sample concentrations using GraphPad Prism 9 software.

$$\% \text{Viability} = (\text{Test OD} / \text{Control OD}) \times 100$$

PSO-NE uptake study

MCF-7 and MDA-MB-231 cells (3×10^5 cells/well) were plated in 35 × 60 mm plates, on sterile cover slips (18 mm round cover slips glasses-Deckgläser) and incubate for 24 h. Following incubation, the cells were subjected to 17 µl of the 1 mg/ml Rhodamine-B loaded PSO-NE and PSO, incubated for duration of 3–4 h, subsequently undergoing 2–3 washes with PBS. The cells underwent fixation using a 4% aqueous solution of paraformaldehyde, followed by washing with PBS, and were subsequently visualized and quantify uptake efficiency using confocal microscopy (Leica DMRE) outfitted with a confocal head TCS-SPE (Leica, Wetzlar, Germany).

Quantification of uptake efficiency:

$$\text{Mean Intensity} = \text{Total Fluorescence Intensity} / \text{Area of ROI } (\mu\text{m}^2) \text{ or Pixels}$$

$$\text{Mean Intensity} = \text{Total Fluorescence Intensity} / \text{Area of ROI } (\mu\text{m}^2) \text{ or Pixels}$$

Total Fluorescence Intensity = sum of all pixel intensities within the ROI (region of interest).

Area = number of pixels or μm^2 in the selected ROI (cell, nucleus, cytoplasm, etc.).

DAPI nuclear morphology assay

In this experiment, both the control and the PSO-NE and PSO treated cells were initially fixed using methanol. Subsequently, DAPI (1 $\mu\text{g}/\text{ml}$) was administered to the cells and incubated at 37 °C for 15 min. The alterations in the structure of the nucleus were analyzed and visualized using confocal microscopy (Leica DMRE) equipped with a confocal head TCS-SPE (Leica, Wetzlar, Germany).

CFSE cell proliferation assay

The examination of cellular proliferation employed CFSE (carboxyl fluorescein diacetate succinimidyl ester), characterized by an excitation maximum at 490 nm and an emission maximum at 520 nm. CFSE establishes a covalent bond with the amino group of the protein, thereby facilitating its application in cytometry for monitoring cell division. To perform this test, the cells were transferred into 15 ml polypropylene tubes and subjected to rinsing 2–3 times with 1X DPBS. The CFSE dye (5 μM) was added to the suspension and incubated at 37 °C for 15 min in a water bath. The sample was subsequently subjected to centrifugation at a velocity of 1000 rpm for duration of 5 min. The supernatant was removed, and the pellet was carefully combined with 10 ml of complete media. The mixture was subsequently subjected to centrifugation, after which the supernatant was carefully extracted. The pellet was meticulously blended and re-suspended in comprehensive media. The CFSE-labeled cells were then placed on a six-well plate and incubate for 24 h. After incubation, cells were treated with PSO-NE and PSO (at IC_{50} concentration) and allowed to incubate for 24 h. Subsequently, the CFSE dye-labeled cells were subjected to cytometry analysis using the BD-LSR II flow Cytometer.

Apoptosis analysis by Annexin-V FITC/PI

MCF-7 and MDA-MB-231 cells were seeded at a density of 1×10^6 cells/ml in 25 cm^2 flasks and incubated for 24 h to allow adherence. Following incubation, cells were treated with PSO-NE and with PSO at the IC_{50} concentration, while untreated cells served as controls. After treatment, both control and treated cells (1×10^6 cells/ml) were harvested and re-suspended in 500 μl of Annexin-V binding buffer. Annexin-V FITC (5 μl) and propidium iodide (5 μl) were added to each tube. The samples were then incubated in the dark at room temperature for 15–20 min. Subsequently, apoptosis analysis was performed using a BD LSR II Flow Cytometer, acquiring 25,000 events per sample. The apoptotic distribution was analyzed using FlowJo_v10 software.

Cell cycle arrest analysis

For this study, cells were seeded at a density of 1×10^6 cells/ml in a 25 cm^2 flask and incubated for 24 h. After incubation, cells were treated with the IC_{50} value of PSO-NE and PSO then again incubated for 24 h. Next, cells were trypsinized and centrifuged at 12,000 rpm for 10 min. Supernatant was discarded, and 70% ethanol (4 ml) was added to the pellet and placed on ice for half an hour for fixation. Next, the cells were centrifuged, and the supernatant was discarded, and the pellet was dissolved in 200 μl of PBS. 50 μg of RNase was added to the suspension and kept it on the ice for half an hour for RNase activity. After that, 5 μl of PI was added and incubated for 5 min. The resulting mixture was then analyzed using the BD-LSR II Flow Cytometer. Each sample captured 25,000 occurrences. Cell cycle arrest was analyzed using FlowJo_v10 software.

Real-time PCR analysis

Total RNA Extraction: Total RNA was isolated from control, PSO-NE and PSO treated MCF-7 and MDA-MB-231 cells at a density of 1×10^6 cells utilizing the Carbunn RNA Purification kit in accordance with the manufacturer's instructions. Cells were treated with the IC_{50} dose of the PSO-NE and incubated for 24 h. The evaluation of RNA concentration and quality was conducted utilising the Nanodrop 2000c Spectrophotometer (Thermo Fisher Scientific), with a focus on the 260/280 ratio.

First-strand cDNA Synthesis: First-strand cDNA was generated from 600 μg of total RNA using a Verso cDNA Kit following the manufacturer's guidelines.

Real-Time PCR reactions: The Real-Time PCR reactions were performed using the SYBR Green PCR kit, along with specific forward and reverse primers for each gene obtained from Integrated DNA Technologies (IDTS). The nucleic acid sequences for the forward (F) and reverse (R) primers targeting the Caspase 3 (Cas3), p53, Bax, Bcl-2, NF- κB , and STAT-3 genes, with GAPDH serving as a housekeeping gene, are detailed in Table 5.

The real-time PCR was conducted with SYBR green dye chemistry on the CFX96 Touch Real-Time PCR Detection System (USA). The 10 μl real-time PCR experiment comprised 5 μl of Maxima SYBR Green qPCR Master Mix (Thermo Fisher Scientific), 0.5 μM of each forward and reverse primer (refer to Table 5), 2 μl of 100-fold diluted cDNA, and nuclease-free water (NFW). The conditions used for the thermal cycler were (i) 95 °C for 5 min (initial denaturation), (ii) 45 cycles at 95 °C for 30 s, 62 °C for 30 s, and 72 °C for 30 s, followed by (iii) melt curve analysis at temperature range of 55–95 °C. The Ct values were calculated via constant threshold value for all the genes studied. The comparative ΔCt ($2^{-\Delta\Delta\text{Ct}}$) method was used for the quantification of comparative gene expression and GAPDH was used as the normalizer gene.

Gene	Primer sequence
p53	F 5'-GTCTATAGGCCACCCC-3'
	R 5'-GCTCGACGCTAGGATCTGAC-3'
Caspase 3	F 5'-TTCAGAGGGGATCGTTGTAGAAGTC-3'
	R 5'-CAAGCTTGTCGGCATACTGTTTCAG-3'
Bax	F 5'-ATGGCTTCTATGAGGCTGAG-3'
	R 5'-CGGCCCCAGTTGAAGTTG-3'
Bcl-2	F 5'-CTGCACCTGACGCCCTTACC-3'
	R 5'-CACATGACCCACCGAACTCAAAGA-3'
STAT-3	F 5'-CATATGCGGCCAGCAAAGAA-3'
	R 5'-ATACCTGCTCTGAAGAACT-3'
NF- κ B	F 5'-ATGGCTTCTATGAGGCTGAG-3'
	R 5'-GTTGTTGTTGGTCTGGATGC-3'
GAPDH	F 5'-GTCTCCTCTGACTTCAACAGCG-3'
	R 5'-ACCACCCTGTTGCTGTAGCCAA-3'

Table5. Primer sequences for real time PCR. F = Forward, R = Reversed.

Statistical analysis

The studies were conducted in three biological and experimental replicates. The GraphPad Prism software (Version 9.0) was used to determine the statistically significant values ($p < 0.05$). An unpaired t-test was used to compare two groups, while a one-way ANOVA Tukeypost test was used to compare three groups. Data is expressed as the mean value \pm S.D ($n = 3$).

Conclusion

The results of this study revealed that a nanoemulsion strategy improved pumpkin seed oil's cytotoxic efficacy against breast cancer cells, inducing cell cycle arrest and apoptosis with minimum effect on normal cells. These promising results highlight the use of PSO-NE as a prospective adjunctive therapy strategy with standard therapies for breast cancer in the years to come. Thus, we recommend PSO-NE as a potent and secure nanoparticle for the treatment of breast cancer in humans. Nevertheless, more investigation is necessary to assess and confirm the safe and cell-dependent anticancer activity, including the examination on other cell lines, and targeted *in-vivo* investigations.

Data availability

The corresponding author is readily available to provide the datasets that were utilized and/or analyzed in this study upon receipt of a reasonable request.

Received: 3 April 2025; Accepted: 17 July 2025

Published online: 30 July 2025

References

1. Wilking, N. et al. 1588MO_PR A comparative study on costs of cancer and access to medicines in Europe. *Ann. Oncol.* **31**, S1197 (2020).
2. Ye, F. et al. Advancements in clinical aspects of targeted therapy and immunotherapy in breast cancer. *Mol. Cancer* **22**(1), 105 (2023).
3. Sung, H. et al. Global cancer statistics 2020: GLOBOCAN estimates of incidence and mortality worldwide for 36 cancers in 185 countries. *CA A Cancer J. Clin.* **71**(3), 209–249 (2021).
4. Li, Y. et al. Global burden of female breast cancer: age-period-cohort analysis of incidence trends from 1990 to 2019 and forecasts for 2035. *Front. Oncol.* **12**, 891824 (2022).
5. Vos, T. et al. Global burden of 369 diseases and injuries in 204 countries and territories, 1990–2019: a systematic analysis for the Global Burden of Disease Study 2019. *The Lancet.* **396**(10258), 1204–1222 (2020).
6. Simu, S. et al. Insights into the behavior of triple-negative mda-mb-231 breast carcinoma cells following the treatment with 17 β -ethinylestradiol and levonorgestrel. *Molecules* **26**(9), 2776 (2021).
7. Keykhasalar, R., Tabrizi, M. H., Ardalan, P. & Khatamian, N. The apoptotic, cytotoxic, and antiangiogenic impact of Linum usitatissimum seed essential oil nanoemulsions on the human ovarian cancer cell line A2780. *Nutr. Cancer* **73**(11–12), 2388–2396 (2021).
8. Kunjiappan, S. et al. Design, in silico modelling and functionality theory of folate-receptor-targeted myricetin-loaded bovine serum albumin nanoparticle formulation for cancer treatment. *Nanotechnology* **31**(15), 155102 (2020).
9. Periasamy, V. S., Athinarayanan, J. & Alshatwi, A. A. Anticancer activity of an ultrasonic nanoemulsion formulation of Nigella sativa L. essential oil on human breast cancer cells. *Ultrason. Sonochem.* **31**, 449–455 (2016).
10. Tomko, A. M., Whynot, E. G., Ellis, L. D. & Dupré, D. J. Anti-cancer potential of cannabinoids, terpenes, and flavonoids present in cannabis. *Cancers* **12**(7), 1985 (2020).
11. Vafayi Malek, A., Karimi, E. & Oskoueian, E. Comparison of antioxidant, antibacterial, and cytotoxic effects of essential oil and nanoemulsion of clove essential oil. *J. Ilam Univ. Med. Sci.* **29**(3), 26–37 (2021).
12. Muchirah, P. N. et al. Characterization and anti-oxidant activity of Cucurbita maxima Duchesne pulp and seed extracts. *J. Phytopharmacol.* **7**(2), 134–140 (2018).
13. Shaban, A. & Sahu, R. P. Pumpkin seed oil: an alternative medicine. *Int. J. Pharmacogn. Phytochem. Res.* **9**(2), 11 (2017).

14. Ito, Y., Maeda, S. & Sugiyama, T. Suppression of 7, 12-dimethylbenz [a] anthracene-induced chromosome aberrations in rat bone marrow cells by vegetable juices. *Mutat. Res. Genetic Toxicol.* **172**(1), 55–60 (1986).
15. Ardabili, G. A., Farhoosh, R. & Haddad Khodaparast, M. Chemical composition and physicochemical properties of pumpkin seeds (*Cucurbita pepo* Subsp. *pepo* Var. *Styriaca*) grown in Iran. *J. Agr. Sci. Tech.* **13**, 1053–1063 (2011).
16. Lozada, M. I. et al. Physicochemical characterization and nano-emulsification of three species of pumpkin seed oils with focus on their physical stability. *Food Chem.* **343**, 128512 (2021).
17. Al Zuhair, H. A., Abd El-Fattah, A. A. & El-Sayed, M. I. Pumpkin-seed oil modulates the effect of felodipine and captopril in spontaneously hypertensive rats. *Pharmacol. Res.* **41**(5), 555–563 (2000).
18. Dreikorn, K. The role of phytotherapy in treating lower urinary tract symptoms and benign prostatic hyperplasia. *World J. Urol.* **19**(6), 426–435 (2002).
19. Nirmala, M. J., Mukherjee, A. & Chandrasekaran, N. Improved efficacy of fluconazole against candidiasis using bio-based microemulsion technique. *Biotechnol. Appl. Biochem.* **60**(4), 417–429 (2013).
20. Abdulsalam, M. M. & Fathy, L. M. Investigation of the apoptotic effect of pumpkin seed oil (*Cucurbita Pepo* l) loaded chitosan nanoparticles on tongue squamous cell carcinoma cell line (scc-25): in-vitro study. *Adv. Dental J.* **6**(4), 721–734 (2024).
21. Amin, M. Z. et al. Comparative assessment of the physicochemical and biochemical properties of native and hybrid varieties of pumpkin seed and seed oil (*Cucurbita maxima* Linn.). *Helvion* **5**(12), e02994 (2019).
22. Nishitani-Yukuyama, M., Tomiko Myiaki Kato, E., Lobenberg, R. & Araci Bou-Chacra, N. Challenges and future prospects of nanoemulsion as a drug delivery system. *Curr. Pharmaceut. Design.* **23**(3), 495–508 (2017).
23. Abadi AV, Karimi E, Oskoueian E, Mohammad GR, Shafaei N. Synthesis, characterization and cytotoxicity evaluation of *Syzygium aromaticum* L. bud (clove) essential oil nanoemulsion (2021).
24. Alshahrani, S. M. A judicious review on the applications of chemotherapeutic loaded nanoemulsions in cancer management. *J. Drug Deliv. Sci. Technol.* **68**, 103085 (2022).
25. Yousefian Rad, E. et al. Citrus lemon essential oil nanoemulsion (CLEO-NE), a safe cell-dependent apoptosis inducer in human A549 lung cancer cells with anti-angiogenic activity. *J. Microencapsul.* **37**(5), 394–402 (2020).
26. Alhakamy, N. A., Fahmy, U. A. & Ahmed, O. A. RETRACTED: attenuation of benign prostatic hyperplasia by optimized tadalafil loaded pumpkin seed oil-based self nanoemulsion: in vitro and in vivo evaluation. *Pharmaceutics*. **11**(12), 640 (2019).
27. Al-Okbi, S. Y., Mohamed, D. A., Hamed, T. E. & Esmail, R. S. Rice bran oil and pumpkin seed oil alleviate oxidative injury and fatty liver in rats fed high fructose diet. *Polish J. Food Nutr. Sci.* **64**(2), 127–133 (2014).
28. Sindi, A. M. & Hosny, K. M. Preparation and evaluation of protective effect of pumpkin seed oil based self nanoemulsifying oral delivery system against ibuprofen-induced peptic ulcer. *J. Drug Deliv. Sci. Technol.* **52**, 415–420 (2019).
29. Abou-Ghali, M. & Stiban, J. Regulation of ceramide channel formation and disassembly: Insights on the initiation of apoptosis. *Saudi J Biol Sci.* **22**(6), 760–772 (2015).
30. Sari, T. P. et al. Preparation and characterization of nanoemulsion encapsulating curcumin. *Food Hydrocolloids* **43**, 540–546 (2015).
31. Perumal, A. B., Li, X., Su, Z. & He, Y. Preparation and characterization of a novel green tea essential oil nanoemulsion and its antifungal mechanism of action against *Magnaporthe oryzae*. *Ultrason. Sonochem.* **76**, 105649 (2021).
32. Marriott, P. J., Shellie, R. & Cornwell, C. Gas chromatographic technologies for the analysis of essential oils. *J. Chromatogr. A* **936**(1–2), 1–22 (2001).
33. Ukwubile, C. A., Ahmed, A., Katsayal, U. A., Ya'u, J. & Mejida, S. GC–MS analysis of bioactive compounds from *Melastoma capitatum* (Vahl) Fern. leaf methanol extract: An anticancer plant. *Sci. African.* **3**, e00059 (2019).
34. Chujo, H., Yamasaki, M., Nou, S., Koyanagi, N., Tachibana, H., & Yamada, K. (2003). Effect of conjugated linoleic acid isomers on growth factor- induced proliferation of human breast cancer cells. *Cancer Lett.* 202(1)
35. Kim, Y.-S., Li, X.-F., Kang, K.-H., Ryu, B. & Kim, S. K. Stigmasterol isolated from marine microalgae *Navicula incerta* induces apoptosis in human hepatoma HepG2 cells. *BMB Rep.* **47**(8), 433 (2014).
36. Wickramasinghe, N. S., Jo, H., McDonald, J. M. & Hardy, R. W. Stearate inhibition of breast cancer cell proliferation: A mechanism involving epidermal growth factor receptor and G-proteins. *Am. J. Pathol.* **148**(3), 987 (1996).
37. Evans, L. M., Cowey, S. L., Siegal, G. P. & Hardy, R. W. Stearate preferentially induces apoptosis in human breast cancer cells. *Nutr. Cancer* **61**(5), 746–753 (2009).
38. Hardy, S. et al. Saturated fatty acid-induced apoptosis in MDA-MB-231 breast cancer cells: a role for cardiolipin. *J. Biol. Chem.* **278**(34), 31861–31870 (2003).
39. Ganesan, K. & Manivel, A. Evaluation of anticancer activity of squalene isolated from *Canthium coromandelicum* leaves. *World J. Pharm. Res.* **7**, 642–648 (2018).
40. Nikolovski, B. G., Ilić, J. D. & Sovilj, M. N. How to formulate a stable and monodisperse water-in-oil nanoemulsion containing pumpkin seed oil: The use of multiobjective optimization. *Braz. J. Chem. Eng.* **33**, 919–931 (2016).
41. Gharibzadeh, S. M. et al. High pressure processing of food-grade emulsion systems: Antimicrobial activity, and effect on the physicochemical properties. *Food Hydrocolloids* **87**, 307–320 (2019).
42. Hasani, F., Pezeshki, A. & Hamishehkar, H. Effect of surfactant and oil type on size droplets of betacarotene-bearing nanoemulsions. *Int. J. Curr. Microbiol. App. Sci.* **4**(9), 146–155 (2015).
43. Tadros, T., Izquierdo, P., Esquena, J. & Solans, C. Formation and stability of nano-emulsions. *Adv. Coll. Interface. Sci.* **108**, 303–318 (2004).
44. Kumar, N. & Mandal, A. Thermodynamic and physicochemical properties evaluation for formation and characterization of oil-in-water nanoemulsion. *J. Mol. Liq.* **266**, 147–159 (2018).
45. Pavoni, L. et al. Properties and stability of nanoemulsions: how relevant is the type of surfactant?. *J. Drug Deliv. Sci. Technol.* **58**, 101772 (2020).
46. Nirmala, M. J., Durai, L., Anusha, G. S. & Nagarajan, R. Nanoemulsion of *Mentha arvensis* essential oil as an anticancer agent in anaplastic thyroid Cancer cells and as an antibacterial agent in *Staphylococcus aureus*. *BioScience*. **11**(4), 1017–1029 (2021).
47. Li, M. & Li, D. Redistribution of mobile surface charges of an oil droplet in water in applied electric field. *Adv. Coll. Interface. Sci.* **236**, 142–151 (2016).
48. Noori, S., Zeynali, F. & Almasi, H. Antimicrobial and antioxidant efficiency of nanoemulsion-based edible coating containing ginger (*Zingiber officinale*) essential oil and its effect on safety and quality attributes of chicken breast fillets. *Food Control* **84**, 312–320 (2018).
49. Kovačević, A. B., Müller, R. H., Savić, S. D., Vuleta, G. M. & Keck, C. M. Solid lipid nanoparticles (SLN) stabilized with polyhydroxy surfactants: Preparation, characterization and physical stability investigation. *Colloids Surf., A* **444**, 15–25 (2014).
50. Ghosh, I., Bose, S., Vippagunta, R. & Harmon, F. Nanosuspension for improving the bioavailability of a poorly soluble drug and screening of stabilizing agents to inhibit crystal growth. *Int. J. Pharm.* **409**(1–2), 260–268 (2011).
51. Zirak, M. B. & Pezeshki, A. Effect of surfactant concentration on the particle size, stability and potential zeta of beta carotene nano lipid carrier. *Int. J. Curr. Microbiol. Appl. Sci.* **4**(9), 924–932 (2015).
52. Nirmala MJ, Durai L, Gopakumar V, Nagarajan R. Preparation of celery essential oil-based nanoemulsion by ultrasonication and evaluation of its potential anticancer and antibacterial activity. *Int. J. Nanomed.* 2020:7651–66.
53. McClements, D. J. Colloidal basis of emulsion color. *Curr. Opin. Colloid Interface Sci.* **7**(5–6), 451–455 (2002).
54. Santos Filho VT, Almeida SA, Mourão SC, Barbosa GM. Development of nanoemulsion containing pumpkin seed oil and minoxidil.
55. Vasquez Mejia CM. Effect of carvacrol-loaded nanoemulsions on a bioluminescent strain of *Escherichia coli* O157: H7.

56. Klang, V., Matsko, N. B., Valenta, C. & Hofer, F. Electron microscopy of nanoemulsions: An essential tool for characterisation and stability assessment. *Micron* **43**(2–3), 85–103 (2012).
57. Alam, A., Ansari, M. J., Alqarni, M. H., Salkini, M. A. & Raish, M. Antioxidant, antibacterial, and anticancer activity of ultrasonic nanoemulsion of *Cinnamomum cassia* L. essential oil. *Plants* **12**(4), 834 (2023).
58. Carpenter, J. & Saharan, V. K. Ultrasonic assisted formation and stability of mustard oil in water nanoemulsion: Effect of process parameters and their optimization. *Ultrason. Sonochem.* **35**, 422–430 (2017).
59. Booyens, J. & Thantsha, M. S. Fourier transform infra-red spectroscopy and flow cytometric assessment of the antibacterial mechanism of action of aqueous extract of garlic (*Allium sativum*) against selected probiotic *Bifidobacterium* strains. *BMC Complement. Altern. Med.* **14**, 1–1 (2014).
60. Banerjee, A., Binder, J., Salama, R. & Trant, J. F. Synthesis, characterization and stress-testing of a robust quillaja saponin stabilized oil-in-water phytocannabinoid nanoemulsion. *J. Cannabis Res.* **3**, 1–4 (2021).
61. Srilatha, R., Aparna, C., Srinivas, P. & Sadanandam, M. Formulation, evaluation and characterization of glipizide nanoemulsion. *Asian J. Pharm. Clin. Res.* **6**(2), 66–71 (2013).
62. Azeem, A. et al. Nanoemulsion components screening and selection: a technical note. *AAPS PharmSciTech* **10**, 69–76 (2009).
63. Al-Balushi, R. A. et al. In vitro anticancer effects of frankincense and its nanoemulsions for enhanced cancer cell targeting. *Front. Pharmacol.* **16**, 1403780 (2025).
64. Nayila, I. et al. Formulation, characterization and evaluation of anti-breast cancer activity of 2-carene nanoemulsion; in silico, in vitro and in vivo study. *Arab. J. Chem.* **17**(9), 105937 (2024).
65. Abd-Rabou, A. A. & Edris, A. E. Frankincense essential oil nanoemulsion specifically induces lung cancer apoptosis and inhibits survival pathways. *Cancer Nanotechnol.* **13**(1), 22 (2022).
66. Guerrero, S. et al. Curcumin-loaded nanoemulsion: A new safe and effective formulation to prevent tumor recurrence and metastasis. *Nanoscale* **10**(47), 22612–22622 (2018).
67. Quignard, S., Frebourg, G., Chen, Y. & Fattaccioli, J. Nanometric emulsions encapsulating solid particles as alternative carriers for intracellular delivery. *Nanomedicine* **11**(16), 2059–2072 (2016).
68. Salehi, F. et al. Apple pectin-based Zataria multiflora essential oil (ZEO) nanoemulsion: An approach to enhance ZEO DNA damage induction in breast cancer cells as in vitro and in silico studies reveal. *Front. Pharmacol.* **13**, 946161 (2022).
69. Zhang, G., Gurtu, V., Kain, S. R. & Yan, G. Early detection of apoptosis using a fluorescent conjugate of annexin V. *Biotechniques* **23**(3), 525–531 (1997).
70. Vundru, S. S., Kale, R. K. & Singh, R. P. β -sitosterol induces G1 arrest and causes depolarization of mitochondrial membrane potential in breast carcinoma MDA-MB-231 cells. *BMC Complement. Altern. Med.* **13**, 1–9 (2013).
71. Gysin, R., Azzi, A. & Visarius, T. γ -Tocopherol inhibits human cancer cell cycle progression and cell proliferation by down-regulation of cyclins. *FASEB J.* **16**(14), 1952–1954 (2002).
72. Banks, H. T. et al. Estimation of cell proliferation dynamics using CFSE data. *Bull. Math. Biol.* **73**, 116–150 (2011).
73. Shanmugapriya, K., Kim, H. & Kang, H. W. In vitro antitumor potential of astaxanthin nanoemulsion against cancer cells via mitochondrial mediated apoptosis. *Int. J. Pharm.* **560**, 334–346 (2019).
74. Alkhatib, M. H., Al-Otaibi, W. A. & Wali, A. N. Antineoplastic activity of mitomycin C formulated in nanoemulsions-based essential oils on HeLa cervical cancer cells. *Chem. Biol. Interact.* **291**, 72–80 (2018).
75. Cheok, C. F. Protecting normal cells from the cytotoxicity of chemotherapy. *Cell Cycle* **11**(12), 2227 (2012).
76. Refaat, A., Abd-Rabou, A. & Reda, A. TRAIL combinations: The new ‘trail’ for cancer therapy. *Oncol. Lett.* **7**(5), 1327–1332 (2014).
77. Flores-Romero, H. et al. BCL-2-family protein tBID can act as a BAX-like effector of apoptosis. *EMBO J.* **41**(2), e108690 (2022).
78. Uba, B. & Muhammad, C. Determination of fatty acid composition and physicochemical properties of Cucurbita maxima (pumpkin) seed oil cultivated in Northeast Nigeria. *East African Scholars Multidiscip. Bull.* **2**(7), 231–234 (2019).
79. Bernardi, D. S. et al. Formation and stability of oil-in-water nanoemulsions containing rice bran oil: in vitro and in vivo assessments. *J. Nanobiotechnol.* **9**(1), 44 (2011).

Acknowledgements

The authors express their gratitude to Jamia Hamdard, New Delhi for its invaluable assistance and provision of the essential research facilities required to carry out the studies. The authors acknowledge the departmental grants by UGC-SAP DRS-I & II and DST-FIST to the Department of Biotechnology, SCLS, Jamia Hamdard, New Delhi, India, for infrastructure and research facilities development. The authors acknowledge financial support by the University Grants Commission, India by providing fellowship to Rupali Ghosh with NTA Ref. No.: 191620149658.

Author contributions

RG worked on data curation, inquiry, formal analysis, validation, and visualization. She also obtained financing and wrote original drafts as well as edits. NF and AV were actively engaged in methodology. Investigation, writing, and editing were all assisted by RG, AR and AV. SW worked on project administration, resources, supervision, validation, visualization, funding acquisition, inquiry, methodology, review, the conception of the idea, work design and editing. Each author reviewed the submitted version of the essay and made contributions to it.

Declarations

Competing interests

The authors declare no competing interest.

Additional information

Supplementary Information The online version contains supplementary material available at <https://doi.org/10.1038/s41598-025-12532-3>.

Correspondence and requests for materials should be addressed to S.W.

Reprints and permissions information is available at www.nature.com/reprints.

Publisher’s note Springer Nature remains neutral with regard to jurisdictional claims in published maps and institutional affiliations.

Open Access This article is licensed under a Creative Commons Attribution-NonCommercial-NoDerivatives 4.0 International License, which permits any non-commercial use, sharing, distribution and reproduction in any medium or format, as long as you give appropriate credit to the original author(s) and the source, provide a link to the Creative Commons licence, and indicate if you modified the licensed material. You do not have permission under this licence to share adapted material derived from this article or parts of it. The images or other third party material in this article are included in the article's Creative Commons licence, unless indicated otherwise in a credit line to the material. If material is not included in the article's Creative Commons licence and your intended use is not permitted by statutory regulation or exceeds the permitted use, you will need to obtain permission directly from the copyright holder. To view a copy of this licence, visit <http://creativecommons.org/licenses/by-nc-nd/4.0/>.

© The Author(s) 2025